Electronic Supplementary Material (ESI) for Energy & Environmental Science.

Rational Design of Flexible-linked 3D Dimeric Acceptors for Stable Organic Solar Cells Demonstrating 19.2% Efficiency

Zhe Zhang[a], Shaohui Yuan[b], Tianqi Chen[b], Jia Wang[b], Yuan-Qiu-Qiang Yi[c], Bin Zhao[d], Miaomiao Li[d], Zhaoyang Yao[a], Chenxi Li[a], Xiangjian Wan[a], Guankui Long[b], Bin Kan[b]*, Yongsheng Chen[a]*

[a] State Key Laboratory and Institute of Elemento-Organic Chemistry, Frontiers Science Center for New Organic Matter, The Centre of Nanoscale Science and Technology and Key Laboratory of Functional Polymer Materials, Renewable Energy Conversion and Storage Center (RECAST), College of Chemistry, Nankai University, Tianjin 300071, China.

[b] School of Materials Science and Engineering, National Institute for Advanced Materials, Nankai University, Tianjin 300350, China.

[c] Division of Nano-Devices Research, Suzhou Institute of Nano-Tech and Nano-Bionics, Chinese Academy of Sciences, Suzhou 215123, China.

[d] School of Materials Science and Engineering, Tianjin Key Laboratory of Molecular Optoelectronic Science, Tianjin University, Tianjin 300072, China.

Contents

1. Materials and Methods.

Polymeric donor PM6, the ending unit 2-(5,6-dichloro-3-oxo-2,3-dihydro-1H-inden-1-ylidene)malononitrile (INCN-2Cl) and 2-(5-bromo-3-oxo-2,3-dihydro-1H-inden-1-ylidene)malononitrile (INCN-Br) were purchased from Solarmer Material (Beijing) Inc, Organtec.Ltd and Woerjiming (Beijing) Technology Development Institute, respectively. Starting material 1 were synthesized according to our previously reported method. All the other reagents and chemicals were purchased from commercial suppliers and used directly without further purification unless otherwise noted. The overall synthetic route and detailed synthesized procedures of CH8-6, CH8-7 and CH8-T and the corresponding characterizations were displayed in "Synthesis of CH8-6, CH8-7 and CH8-T" below.

Computational methods in this work. The structures were subsequently optimized with Density Functional Theory (DFT) in vacuum within the Gaussian 16 software. The structure optimization, frequency analysis and energy level of frontier molecular orbital were obtained at the Becke three-parameter Lee-Yang-Parr (B3LYP) hybrid functional with the 6-31G(d) basis set.

UV-visible (UV-*Vis*) absorption. UV-vis absorption spectra were recorded on a Cary 5000 UV-vis spectrophotometer.

Electrochemical characterizations. The cyclic voltammetry (CV) was performed on a LK98B II Microcomputer-based Electrochemical Analyzer using a glassy carbon electrode as the working electrode, a saturated calomel electrode (SCE) as reference electrode, and a Pt wire as the counter electrode. The sample film on working electrode was in an acetonitrile solution of 0.1 mol L^{-1} n-Bu_4NPF_6 at a scan rate of 100 mV s^{-1}. The ferrocene/ferrocenium was employed as internal reference. The HOMO and LUMO levels were calculated using the following equations: E_{HOMO}=-(E_{ox}+4.8-E_{Fc/Fc^+}) eV, E_{LUMO}=-(E_{red}+4.8-E_{Fc/Fc^+}) eV.

Photoluminescence (PL). Temperature-dependent PL spectra varied from 140 to 300 K were measured were conducted by using FLS1000 equipment. The emission spectra of CH8-6, CH8-7 and CH8-T were obtained using the same setup used for recording

electroluminescence spectra excited by an 820 nm wavelength provided by Xenon lamp. (Detector for NIR 5509 PMT, 600-1700 nm). The E_a values were obtained by fitting the temperature-varying PL intensities:

$$I(T) = \frac{I_0}{1 + Ae^{-\frac{E_a}{k_B T}}}$$

where I_0 is the intensity at 0 K, k_B is the Boltzmann constant, T is the temperature.

EQE_{EL} and FTPS-EQE. The OSCs used for the FTPS-EQE spectra measurements are the same with those of the *J-V* measurements, with a conventional device structure of ITO/PEDOT:PSS/Active layer/PNDIT-F3N/Ag. EQE_{EL} measurements were performed by applying external voltage/current sources through the devices (REPS, Enlitech). The FTPS-EQE measurement was carried out on an Enlitech FTPS PECT-600 instrument.

Measurements of Transient Photocurrent (TPC). The TPC measurements were performed on a Molex 180081-4320 with a light intensity of about 0.5 sun. Voltage and current dynamics were recorded on a digital oscilloscope (Tektronix MDO4104C), and voltages at open circuit and currents under short circuit conditions were measured over a 50 Ω resistor, respectively.

Atomic force microscopy (AFM). The AFM images were obtained from a Bruker Dimension Icon atomic force microscope by using in tapping mode. The film samples were prepared under the same conditions as those used for device fabrication.

Grazing incidence wide angle X-ray scattering (GIWAXS). The GIWAXS data was obtained at in a Xeuss 3.0 SAXS/WAXS system with a wavelength of λ = 1.341 Å at Vacuum Interconnected Nanotech Workstation (Nano-X). The exposure time was 10 minutes. The film samples on the Si substrate were prepared under the same conditions as those used for device fabrication.

Contact angles. The contact angles were measured using a JC2000D1 contact angle instrument.

Surface tension characterization. The surface tension of the neat films could be

estimated according to the Wu's model:

$$\gamma_{water}(1+cos\theta_{water}) = \frac{4\gamma_{water}^{d}\gamma^{d}}{\gamma_{water}^{d}+\gamma^{d}} + \frac{4\gamma_{water}^{p}\gamma^{p}}{\gamma_{water}^{p}+\gamma^{p}}$$

$$\gamma_{EGL}(1+cos\theta_{EGL}) = \frac{4\gamma_{EGL}^{d}\gamma^{d}}{\gamma_{EGL}^{d}+\gamma^{d}} + \frac{4\gamma_{EGL}^{p}\gamma^{p}}{\gamma_{EGL}^{p}+\gamma^{p}}$$

$$\gamma = \gamma^{d} + \gamma^{p}$$

where θ refers to the contact angle of each thin film and γ is the surface tension of the materials, which is equal to the sum of the dispersion (γ^{d}) and polarity (γ^{p}) components; γ_{water} and γ_{EGL} are the surface tensions of the water and ethylene glycol; γ_{water}^{d}, γ_{EGL}^{d}, γ_{water}^{p} and γ_{EGL}^{p} are the dispersion and polarity components of γ_{water} and γ_{EGL}, respectively.

Mechanical characterizations of blend films. For film-on-elastomer (FOE) measurements, poly(dimethylsiloxane) (PDMS) (base:crosslinker = 10:1 w/w) was chosen as the elastomer substrate. Polystyrene sulfonic acid (PSS) sacrificial layer was spin coated on glass substrate at 3000 rpm for 40 s followed by thermal annealing at 140 ℃ for 20 mins. Afterwards, the semiconductor layers were spin coated on the top of PSS to form thin films with the thickness of ~120 nm. The PM6:CH8-6, PM6:CH8-7 and PM6:CH8-T blend films were prepared under the same conditions as the optimal OSC devices. Then the glass substrates with PSS and polymer films were immersed into water and the floating polymer film was transferred to PDMS elastomer substrates. Crack onset strain (COS) was observed in situ under the POM.

Device fabrication and measurement. The conventional devices were fabricated with an architecture of ITO/PEDOT:PSS (4083)/PM6: Acceptors/PNDIT-F3N/Ag. In detail, the ITO glass was pre-cleaned in turn in an ultrasonic bath of detergent, deionized water, acetone and isopropanol. Then the surface of ITO was treated by UV light in an ultraviolet-ozone chamber (Jelight Company) for 15 min. A thin layer of PEDOT: PSS was deposited on the ITO substrate by spin-coating a PEDOT:PSS solution (Baytron P VP AI 4083) at 4300 rpm for 20 s and then dried at 150 ℃ for 20 mins in air. Then the

substrates were transferred to a glovebox filled with nitrogen. The blends with solid additives were fully dissolved in chloroform (CF) at a concentration of 6 mg/mL of PM6. The resulting solutions were stirred at room temperature for 6 hours and then spin-casted at 2000 rpm for 30 s onto the PEDOT:PSS layer. For ternary devices, the concentration of PM6 was also settled as 6 mg/mL, and the PM6:CH8-6:L8-BO solution (1:1:0.3 by weight) were stirred at room temperature for 6 hours before coating on the ITO/PEDOT:PSS substrate. Then the films were treated with the thermal annealing at 90˚C for 10 min. The thickness of all active layers was controlled to be ~100 nm. After that, a thin layer of PNDIT-F3N (dissolved in methanol with the concentration of 1 mg/mL) was spin-coated on the top of the active layer. Finally, a layer of Ag with thickness of 150 nm was deposited under 2×10^{-6} Pa. The active area of the device was 0.04 cm^2.

The glue dispenser/spin coater (Brand-REESEEN, PvS-mini7) used in the lab are from Jiangyin J. Wanjia Technology Co., Ltd.

The current density-voltage (*J-V*) curves of photovoltaic devices were recorded by a Keithley 2400 source-measure unit. The photocurrent was measured under the simulated illumination of 100 mW cm^{-2} with AM1.5 G using a Enli SS-F5-3A solar simulator, which was calibrated by a standard Si solar cell (made by Enli Technology Co., Ltd., Taiwan, and calibrated report can be traced to NREL). The thickness of the active layers was measured by a Veeco Dektak 150 profilometer. The EQE spectra were measured by using a QE-R Solar Cell. Response Measurement System (Enli Technology Co., Ltd., Taiwan).

OPV flexible device fabrication. The flexible device was fabricated following the same route of rigid device except that the substrate was replaced by PEN (polyethylene naphthalate)/ITO flexible substrate.

Space-charge-limited current (SCLC) measurement. The SCLC method was used to measure the hole and electron mobilities, by using a diode configuration of ITO /PEDOT:PSS/active layer/MoO_3/Al for hole-only device and ITO/ZnO/active layer/ PNDIT-F3N/Al for electron-only device. In our case, we applied forward scans for all

the SCLC measurements, and hence the ITO and Al electrodes should be the anode and cathode, respectively. The dark current density curves were recorded with a bias voltage in the range of 0-8 V. The mobilities were estimated by taking current-voltage curves and fitting the results based on the equation listed below:

$$J = \frac{9\varepsilon_0\varepsilon_\gamma\mu V^2}{8L^3}$$

where J is the current density, ε_0 is the vacuum permittivity, ε_r is the relative dielectric constant, μ is the mobility, and L is the film thickness. V ($=V_{app} - V_{bi}$) is the internal voltage in the device, where V_{app} is the applied voltage to the device and V_{bi} is the built-in voltage due to the relative work function difference of the two electrodes.

2. Synthesis of CH8-6, CH8-7 and CH8-T.

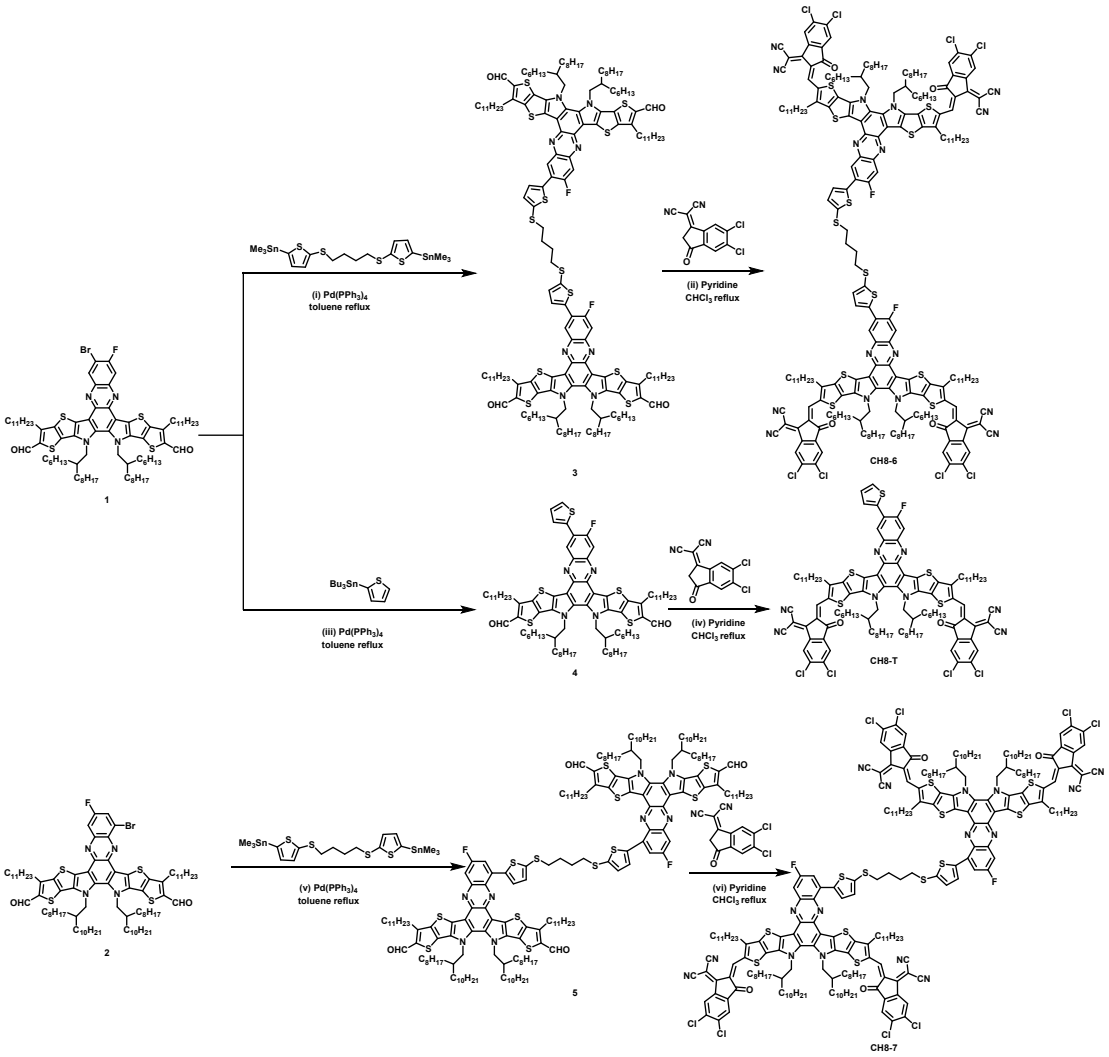

Scheme S1. The overall synthetic route to CH8-6, CH8-7 and CH8-T. Reagents and conditions: (i) $Pd(PPh_3)_4$, 1,4-bis((5-(trimethylstannyl)thiophen-2-yl)thio)butane, toluene, reflux; (ii) 2-(5,6-dichloro-3-oxo-2,3-dihydro-1H-inden-1-ylidene)malononitrile, pyridine, $CHCl_3$, reflux; (iii) $Pd(PPh_3)_4$, tributyl(thiophen-2-yl)stannane, toluene, reflux; (iv) 2-(5,6-dichloro-3-oxo-2,3-dihydro-1H-inden-1-ylidene)malononitrile, pyridine, $CHCl_3$, reflux; (v) $Pd(PPh_3)_4$, 1,4-bis((5-(trimethylstannyl)thiophen-2-yl)thio)butane, toluene, reflux; (vi) 2-(5,6-dichloro-3-oxo-2,3-dihydro-1H-inden-1-ylidene)malononitrile, pyridine, $CHCl_3$, reflux.

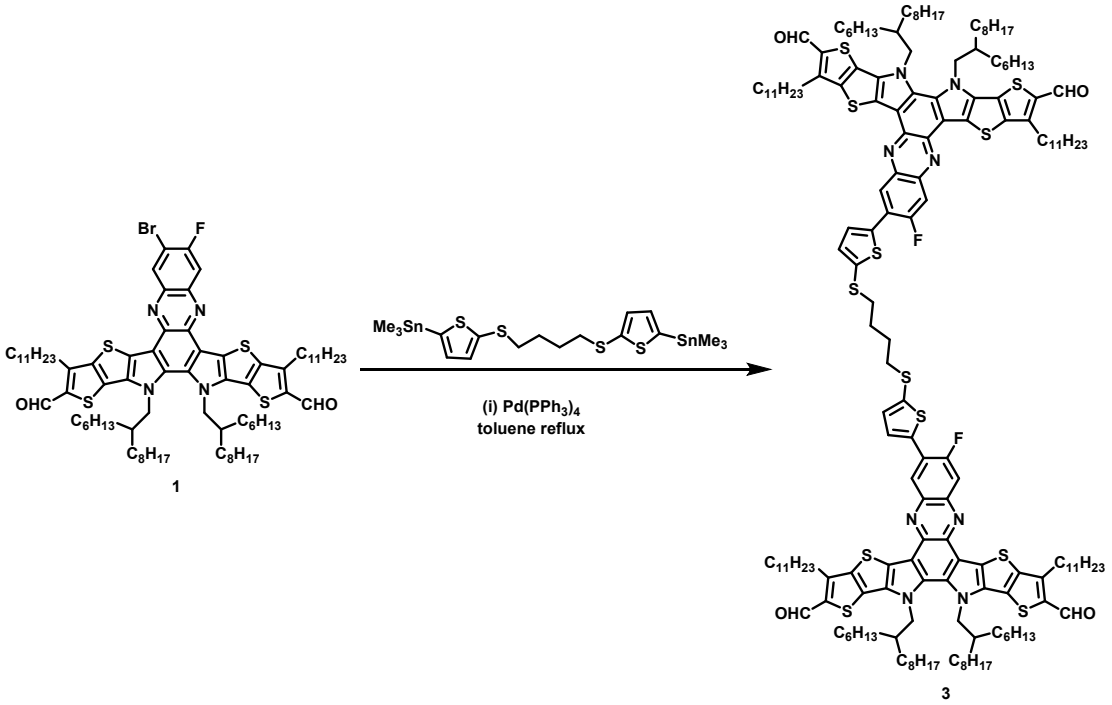

Scheme S2. Synthesis of compound 3. The key compound **1** was synthesized according to our previous report. Compound **1** (300 mg, 215 μmol, 1.0 eq.), 1,4-bis((5-(trimethylstannyl)thiophen-2-yl)thio)butane (66 mg, 108 μmol, 0.5 eq.), $Pd(PPh_3)_4$ (50 mg, 43 μmol, 0.2 eq.), and 30 mL toluene was added to 100 mL two-necked round bottom flask. The flask was purged with argon and sealed under argon flow. The resulting mixture was stirred and heated to reflux for 12 h. Then the mixture was allowed to warm to room temperature, and extracted with chloroform (3×75 mL). The combined organic phase was dried over Na_2SO_4, filtrated, and concentrated under vacuum. The crude product was purified by column chromatography on silica gel with petroleum ether/dichloromethane (*v*/*v* = 2/3) as the eluent to give compound **3** as a red solid (146 mg, 47%). ^{1}H NMR (400 MHz, $CDCl_3$) δ 10.14 (s, 2H), 10.14 (s, 2H), 8.54 (d, *J*=7.5 Hz, 2H), 7.95 (d, *J*=11.8 Hz, 2H), 7.66 (s, 2H), 7.26 (s, 2H), 4.70 (s, 8H), 3.22 (d, *J*=6.9 Hz, 8H), 3.01 (s, 4H), 2.16 (s, 4H), 1.95 (s, 8H), 1.50 (s, 8H), 1.40 (s, 8H), 1.31-1.24 (m, 64H), 1.13-1.08 (m, 16H), 1.02-0.93 (m, 54H), 0.88-0.83 (m, 22H), 0.80-0.74 (m, 16H), 0.69-0.64 (m, 12H). ^{13}C NMR (101 MHz, $CDCl_3$) δ 181.84, 160.65, 158.12, 146.92, 144.34, 141.37, 141.24, 139.75, 138.88, 138.52, 138.43, 137.27, 136.91, 136.76, 133.95, 133.01, 132.72, 130.13, 129.85, 129.62, 129.53, 128.44,

128.20, 127.83, 125.98, 125.80, 117.96, 117.89, 113.15, 113.00, 55.61, 39.09, 38.33, 32.03, 31.88, 31.69, 30.70, 30.61, 29.84, 29.81, 29.72, 29.57, 29.44, 29.26, 28.35, 25.71, 22.81, 22.64, 22.54, 14.25, 14.19, 14.02. MS (m/z, MALDI): Calc. for $[C_{220}H_{252}Cl_8F_2N_{16}O_4S_{12}]^+$ 2910.6128, found: 2910.5870.

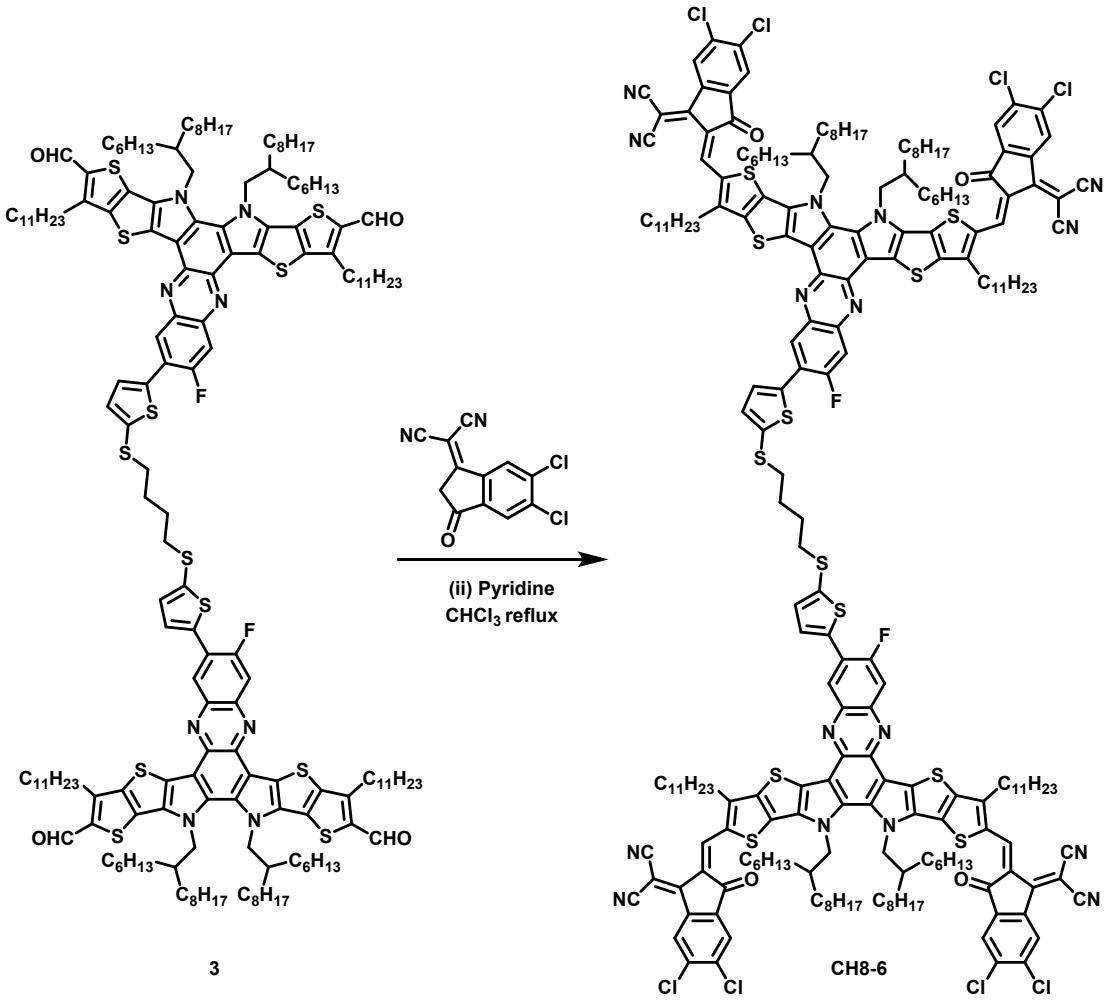

Scheme S3. Synthesis of compound CH8-6. Under argon protection, compound **3** (140 mg, 48 μmol, 1.0 eq.), 2-(5,6-dichloro-3-oxo-2,3-dihydro-1H-inden-1-ylidene)malononitrile (152 mg, 577 μmol, 12 eq.) and 30 mL dry chloroform were added to 100 mL two-necked round bottom flask. Then 0.5 mL pyridine was dropped into the mixture. The reaction mixture was stirred at 80 ℃ for 12 h. After cooling to room temperature, the reaction mixture was precipitated in 75 mL methanol. The precipitate was purified by column chromatography on silica gel with petroleum ether/ chloroform (v/v=5/4) as eluent to give black compound **CH8-6** (102 mg, 55%). ^{1}H NMR (400 MHz, $CDCl_3$) δ 9.22 (s, 2H), 8.86 (s, 2H), 8.81 (s, 2H), 8.43 (s, 2H), 8.08

(s, 2H), 8.05 (s, 2H), 7.98 (s, 2H), 7.57 (s, 2H), 7.28 (d, *J*=3.6 Hz, 2H), 4.98 (s, 4H), 4.87 (s, 4H), 3.27 (s, 4H), 3.10 (s, 8H), 3.01 (s, 4H), 2.52 (s, 2H), 2.28 (s, 2H), 2.09 (s, 4H), 1.93 (s, 4H), 1.71 (s, 4H), 1.64-1.56 (m, 6H), 1.50-1.38 (m, 20H), 1.35-1.14 (m, 86H), 1.13-0.97 (m, 42H), 0.96-0.90 (m, 4H), 0.88-0.77 (m, 14H), 0.75-0.54 (m, 24H). Calc. for $[C_{220}H_{252}Cl_8F_2N_{16}O_4S_{12}]^+$ 3890.8608, found: 3891.4201.

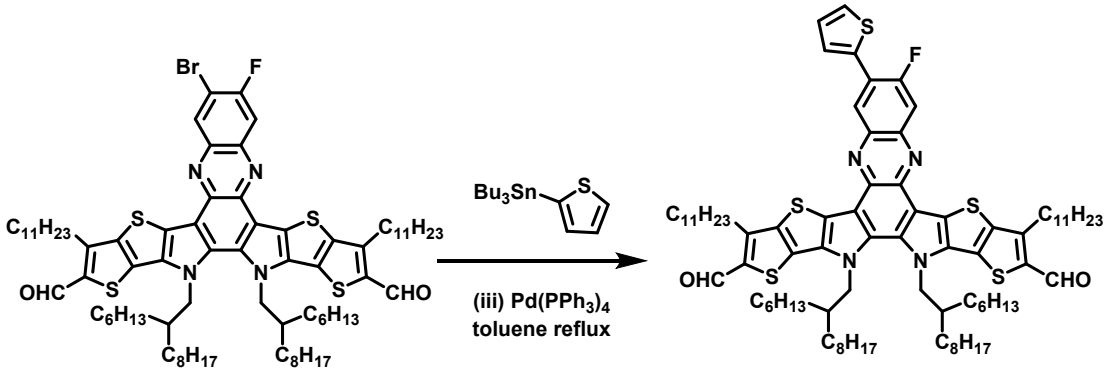

Scheme S4. Synthesis of compound 4. Compound **1** (200 mg, 144 μmol, 1.0 eq.), tributyl(thiophen-2-yl)stannane (27 mg, 72 μmol, 0.5 eq.), $Pd(PPh_3)_4$ (33 mg, 29 μmol, 0.2 eq.), and 30 mL toluene was added to 100 mL two-necked round bottom flask. The flask was purged with argon and sealed under argon flow. The resulting mixture was stirred and heated to reflux for 12 h. Then the mixture was allowed to warm to room temperature, and extracted with chloroform (3×75 mL). The combined organic phase was dried over Na_2SO_4, filtrated, and concentrated under vacuum. The crude product was purified by column chromatography on silica gel with petroleum ether/dichloromethane (*v*/*v* = 1/1) as the eluent to give compound **4** as a red solid (157 mg, 78%). ^{1}H NMR (400 MHz, $CDCl_3$) δ 10.15 (s, 2H), 8.59 (d, *J*=8.0 Hz, 1H), 8.06 (d, *J*=12.0 Hz, 1H), 7.77 (s,1H), 7.50 (d, *J*=4.9 Hz, 1H), 7.24-7.16 (m, 1H), 4.70 (d, *J*=6.9 Hz, 4H), 3.22 (t, *J*=7.3 Hz, 4H), 2.16 (s, 2H), 2.04-1.83 (m, 4H), 1.55-1.48 (m, 4H), 1.47-1.20 (m, 34H), 1.20-1.07 (m, 14 H), 1.06-0.91 (m, 34 H), 0.90-0.79 (m, 12H), 0.79-0.74 (m, 6H), 0.71-0.64 (m, H). ^{13}C NMR (101 MHz, $CDCl_3$) δ 181.83, 160.79, 158.24, 147.05, 144.33, 141.39, 141.25, 139.00, 138.39, 138.33, 138.31, 136.87, 136.82, 136.80, 132.99, 132.71, 129.64, 128.26, 128.18, 128.09, 128.01, 127.95, 127.89, 127.24, 127.21, 126.47, 126.29, 118.00, 117.84, 113.18, 112.95, 77.48, 77.16,

76.84, 55.47, 39.16, 39.13, 32.03, 31.87, 31.69, 30.73, 30.65, 30.57, 29.88, 29.84, 29.80, 29.76, 29.75, 29.70, 29.58, 29.55, 29.46, 29.44, 29.26, 28.30, 25.70, 22.81, 22.68, 22.58, 14.23, 14.19, 14.06. MS (m/z, MALDI): Calc. for $[C_{84}H_{119}FN_4O_2S_5]^+$ 1396.2004, found: 1395.7939.

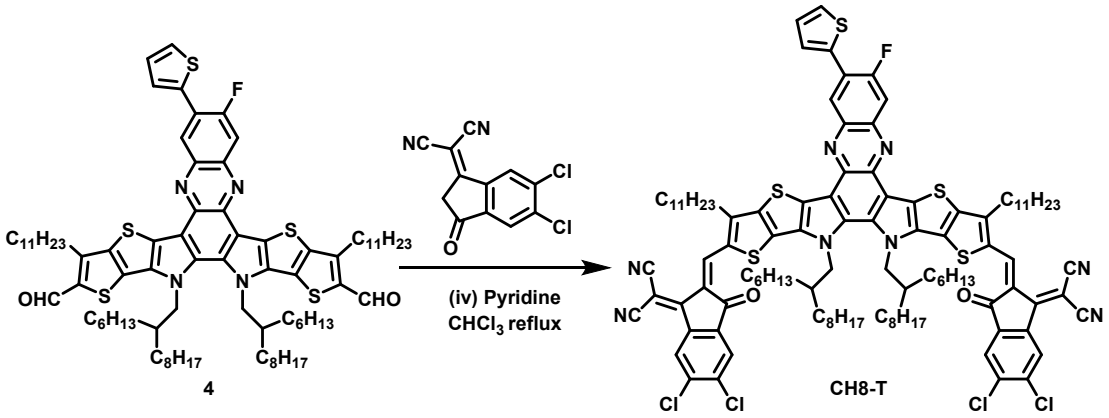

Scheme S5. Synthesis of compound CH8-T. Under argon protection, compound **4** (130 mg, 93 μmol, 1.0 eq.), 2-(5,6-dichloro-3-oxo-2,3-dihydro-1H-inden-1-ylidene)malononitrile (98 mg, 372 μmol, 4.0 eq.), and chloroform (40 mL) was added to 100 mL two-necked round bottom flask. After adding dry pyridine (0.5 mL), the reaction mixture was further allowed to stir at 75 ºC for 12 hours. After cooling to room temperature, the mixture solution was poured into methanol (100 mL) and filtered. The precipitate was purified by column chromatography on silica gel with petroleum ether/ chloroform (*v*/*v*=1/1) as eluent to afford compound **CH8-T** (96 mg, 55%). ^{1}H NMR (400 MHz, $CDCl_3$) δ 9.17 (s, 2H), 8.78 (d, *J*=4.6 Hz, 2H), 8.57 (d, *J*=8.0 Hz, 1H), 8.04 (d, *J*=11.6 Hz, 1H), 7.98 (d, *J*=2.4 Hz, 1H), 7.80 (s,1H), 7.51 (d, *J*=5.2 Hz, 1H), 7.24-7.19 (m, 1H), 4.83 (d, *J*=7.5 Hz, 4H), 3.26 (d, *J*=7.3 Hz, 4H), 2.24 (s, 2H), 1.90 (s, 4H), 1.59-1.53 (m, 4H), 1.44-1.35 (m, 6H), 1.34-1.16 (m, 32H), 1.14-0.98 (m, 34H), 0.93-0.82 (m, 10H), 0.77-0.71 (m, 6H), 0.71-0.65 (m, 6H). Calc. for $[C_{108}H_{123}Cl_4FN_8O_2S_5]^+$ 1886.3244, found: 1885.7143.

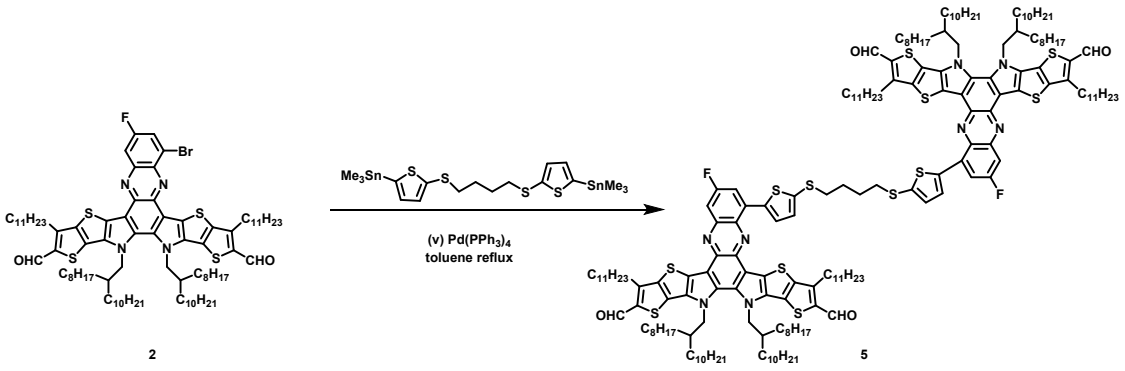

Scheme S6. Synthesis of compound 5. Compound **2** (350 mg, 232 μmol, 1.0 eq.), 1,4-bis((5-(trimethylstannyl)thiophen-2-yl)thio)butane (71 mg, 116 μmol, 0.5 eq.), $Pd(PPh_3)_4$ (53 mg, 46 μmol, 0.2 eq.), and 30 mL toluene was added to 100 mL two-necked round bottom flask. The flask was purged with argon and sealed under argon flow. The resulting mixture was stirred and heated to reflux for 12 h. Then the mixture was allowed to warm to room temperature, and extracted with chloroform (3×75 mL). The combined organic phase was dried over Na_2SO_4, filtrated, and concentrated under vacuum. The crude product was purified by column chromatography on silica gel with petroleum ether/dichloromethane (*v*/*v* = 2/3) as the eluent to give compound **5** as a red solid (154 mg, 42%).^{1}H NMR (400 MHz, $CDCl_3$) δ 10.15 (s, 2H), 10.12 (s, 2H), 7.91-7.82 (m, 6H), 7.30 (d, *J*=3.3Hz, 2H), 4.69 (s, 8H), 3.23 (d, *J*=3.3Hz, 8H),3.00 (s, 4H), 2.12 (s, 4H), 1.50 (s, 8H), 1.33-1.17 (m, 82H), 1.13-1.04 (m, 38H), 0.97-0.71 (m, 108H). ^{13}C NMR (101 MHz, $CDCl_3$) δ 181.82, 181.74, 163.17, 160.64, 146.99, 146.93, 144.40, 144.08, 142.78, 140.96, 138.65, 137.87, 137.16, 137.00, 136.68, 135.51, 134.49, 133.33, 132.90, 129.61, 129.42, 128.43, 128.26, 127.82, 118.04, 117.72, 117.33, 117.03, 111.70, 111.48, 55.50, 39.10, 39.06, 38.34, 32.03, 32.00, 31.88, 31.56, 30.76, 30.69, 30.59, 30.50, 29.96, 29.83, 29.70, 29.65, 29.55, 29.47, 29.39, 29.28, 28.65, 28.40, 28.33, 25.69, 25.64, 22.79, 22.68, 14.23, 14.18. MS (m/z, MALDI): Calc. for $[C_{188}H_{276}F_2N_8O_4S_{12}]^+$ 3135.0448, found: 3134.8377.

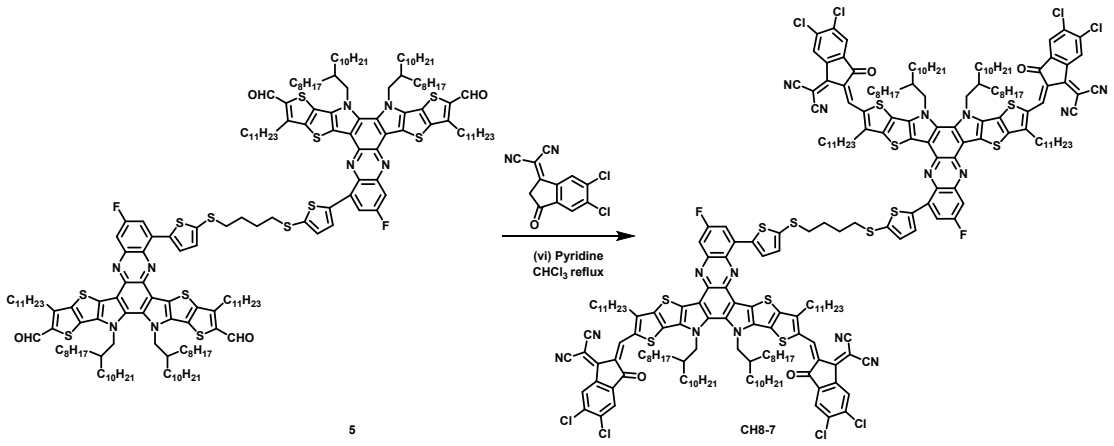

Scheme S7. Synthesis of compound CH8-7. Under argon protection, compound **5** (120 mg, 38 μmol, 1.0 eq.), 2-(5,6-dichloro-3-oxo-2,3-dihydro-1H-inden-1-ylidene)malononitrile (121 mg, 459 μmol, 12 eq.) and 30 mL dry chloroform were added to 100 mL two-necked round bottom flask. Then 0.5 mL pyridine was dropped into the mixture. The reaction mixture was stirred at 80 ℃ for 12 h. After cooling to room temperature, the reaction mixture was precipitated in 75 mL methanol. The precipitate was purified by column chromatography on silica gel with petroleum ether/ chloroform (v/v=1/1) as eluent to give black compound **CH8-7** (91 mg, 58%). ^{1}H NMR (400 MHz, $CDCl_3$) δ 9.01 (s, 4H), 8.65 (s, 4H), 8.05 (s, 2H), 7.88-7.60 (m, 6H), 7.18 (s, 4H), 4.90 (s, 8H), 3.20 (s, 8H), 3.04 (s, 4H), 2.40 (s, 4H), 1.50 (s, 8H), 2.00 (s, 4H), 1.83 (s, 8H), 1.58-1.49 (m, 12H), 1.43-1.23 (m, 72H), 1.21-1.16 (m, 20H). 1.14-1.00 (m, 86H), 0.88-0.69 (m, 38H). MS (m/z, MALDI): Calc. for $[C_{236}H_{284}Cl_8F_2N_{16}O_4S_{12}]^+$ 4115.2928, found: 4115.6715.

3. Figures and tables

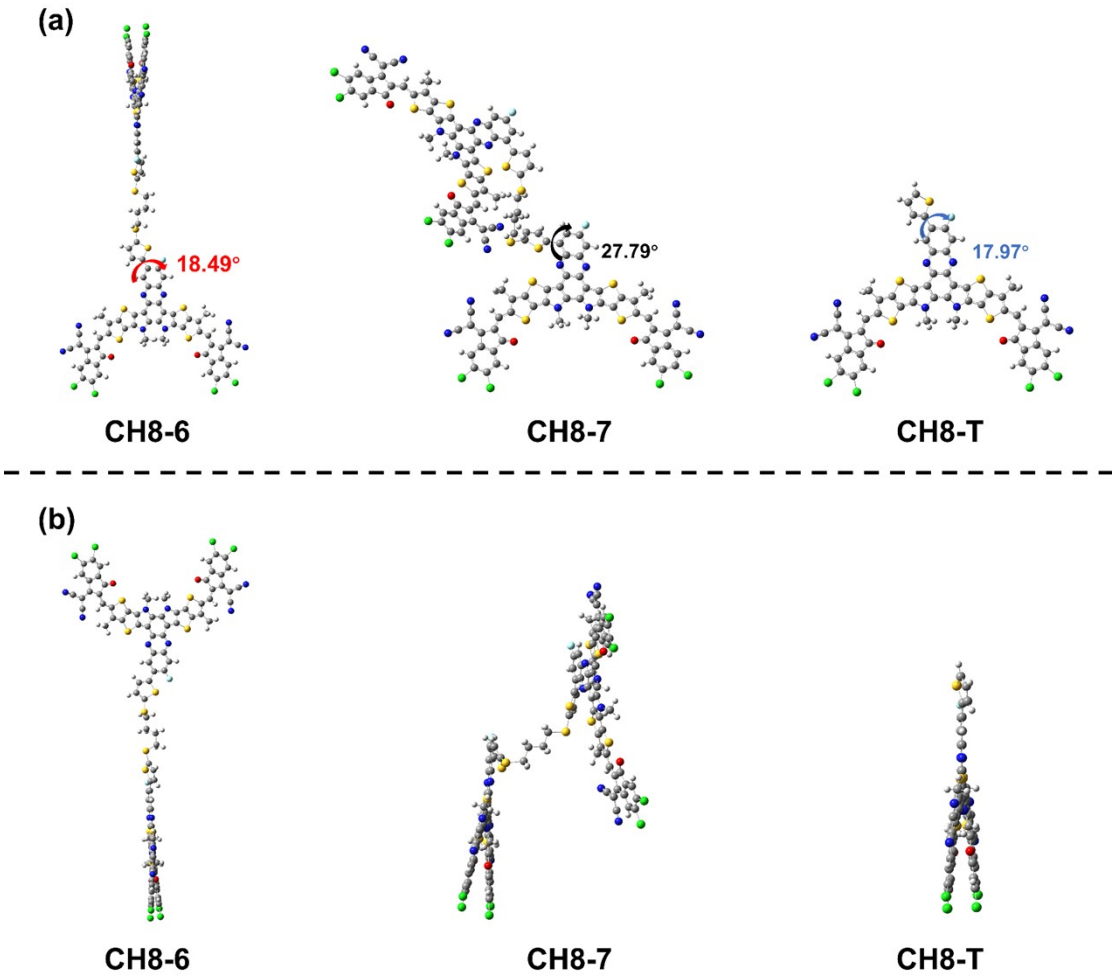

Figure S1. (a) The optimized molecular structures of CH8-6, CH8-7 and CH8-T by a DFT method in front view; (b) The optimized molecular structures of CH8-6, CH8-7 and CH8-T by a DFT method in side view.

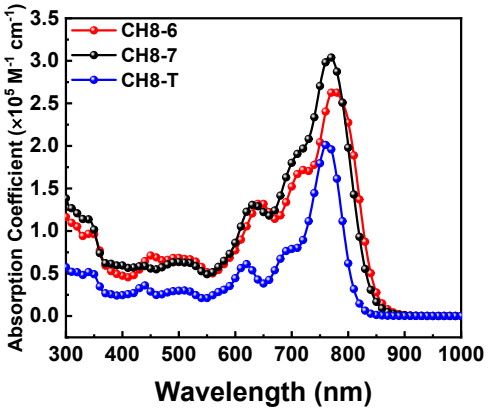

Figure S2. UV-vis absorption spectra of CH8-6, CH8-7 and CH8-T in chloroform solutions.

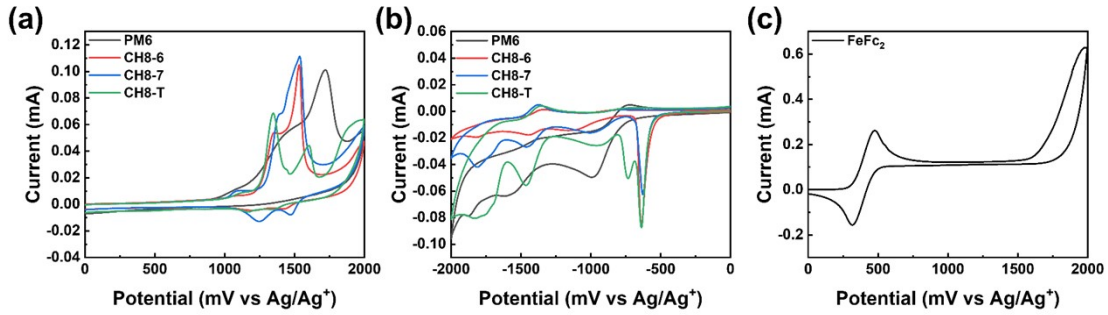

Figure S3. (a) Cyclic voltammograms of the oxidation of PM6, CH8-6, CH8-7 and CH8-T films; (b) Cyclic voltammograms of the reduction of PM6, CH8-6, CH8-7 and CH8-T films; (c) Cyclic voltammogram of ferrocene.

Table S1. Photovoltaic performance of the solar cells based on **PM6**:**CH8-6** with different D:A ratios under the illumination of AM 1.5G.

	D:A	*V*oc (V)	J_{sc} (mA cm^{-2})	FF (%)	PCE (%)
PM6:CH8-6	1:1	0.897	25.22	67.2	15.21
	1:1.2	0.895	25.48	67.9	15.47
	1:1.4	0.894	24.76	65.4	14.49

Table S2. Photovoltaic performance of the solar cells based on **PM6**:**CH8-7** with different D:A ratios under the illumination of AM 1.5G.

	D:A	*V*oc (V)	J_{sc} (mA cm^{-2})	FF (%)	PCE (%)
PM6:CH8-7	1:1	0.911	23.66	72.7	15.68
	1:1.2	0.915	24.31	71.5	15.91
	1:1.4	0.905	24.34	68.1	15.02

Table S3. Photovoltaic performance of the solar cells based on **PM6**:**CH8-T** with different D:A ratios under the illumination of AM 1.5G.

	D:A	*V*oc (V)	J_{sc} (mA cm^{-2})	FF (%)	PCE (%)
PM6:CH8-T	1:1	0.905	25.19	63.8	14.53
	1:1.2	0.903	25.10	65.4	14.79
	1:1.4	0.895	25.45	63.6	14.45

Table S4. Photovoltaic performance of the solar cells based on **PM6**:**CH8-6** (1:1.2, w/w) with different 2,5-dichloro-3,4-diiodothiophene (SA-T5) contents under the illumination of AM 1.5G.

	wt (%)	TA	V_{oc} (V)	J_{sc} (mA cm^{-2})	FF (%)	PCE (%)
PM6:CH8-6 1:1.2	50	90 ℃-8 min	0.888	26.17	74.3	17.20
	75	90 ℃-8 min	0.891	26.23	77.8	18.19
	100	90 ℃-8 min	0.896	26.14	75.6	17.63

Table S5. Photovoltaic performance of the solar cells based on **PM6**:**CH8-7** (1:1.2, w/w) with different 2,5-dichloro-3,4-diiodothiophene (SA-T5) contents under the illumination of AM 1.5G.

	wt (%)	TA	V_{oc} (V)	J_{sc} (mA cm^{-2})	FF (%)	PCE (%)
PM6:CH8-7 1:1.2	50	90 ℃-8 min	0.897	24.85	77.2	17.2
	75	90 ℃-8 min	0.904	24.97	78.3	17.7
	100	90 ℃-8 min	0.892	24.80	77.2	17.2

Table S6. Photovoltaic performance of the solar cells based on **PM6**:**CH8-T** (1:1.2, w/w) with different 2,5-dichloro-3,4-diiodothiophene (SA-T5) contents under the illumination of AM 1.5G.

	wt (%)	TA	V_{oc} (V)	J_{sc} (mA cm^{-2})	FF (%)	PCE (%)
PM6:CH8-T 1:1.2	50	90 ℃-8 min	0.875	25.48	72.8	16.2
	75	90 ℃-8 min	0.869	25.92	75.4	17.0
	100	90 ℃-8 min	0.863	25.00	74.8	16.2

Table S7. Photovoltaic performances of the solar cells based on **PM6**:**CH8-6:L8-BO** with different CH8-6:L8-BO ratios under the illumination of AM 1.5G.

PM6:CH8-6:L8-BO	V_{oc} (V)	J_{sc} (mA cm^{-2})	FF (%)	PCE (%)
1:1.2:0	0.891	26.23	77.8	18.2
1:1.1:0.2	0.878	27.16	78.2	18.6
1:1:0.3	0.882	27.63	78.6	19.2
1:0.9:0.4	0.884	27.38	77.0	18.6

Table S8. Total energy loss values and different contributions in organic solar cells based on the SQ limit theory.

Device	E_g[a] (eV)	V_{oc} (V)	$V_{oc,sq}$[b] (V)	$V_{oc,rad}$[c] (V)	ΔE_1 (eV)	ΔE_2 (eV)	ΔE_3[d] (eV)	ΔE_3[e] (eV)	E_{loss} (eV)
PM6: CH8-6	1.399	0.891	1.136	1.073	0.263	0.063	0.182	0.187	0.508
PM6: CH8-7	1.422	0.904	1.157	1.107	0.265	0.050	0.203	0.202	0.518
PM6:CH8-T	1.366	0.869	1.145	1.066	0.261	0.039	0.197	0.193	0.497

[a]. E_g was determined by FTPS-EQE spectra of devices; [b]. $V_{oc,sq}$ is calculated according to the SQ limit; [c]. $V_{oc,rad}$ is the V_{oc} when there is only radiative recombination and is calculated from the EQE, FTPS-EQE and EL measurements; [d]. ΔE_3 was calculated by $q(V_{oc,rad}\text{-}V_{oc})$; [e]. ΔE_3 was obtained from the equation $q\Delta V_{nr} = -kT\text{InEQE}_{EL}$ by measuring the device EQE_{EL}.

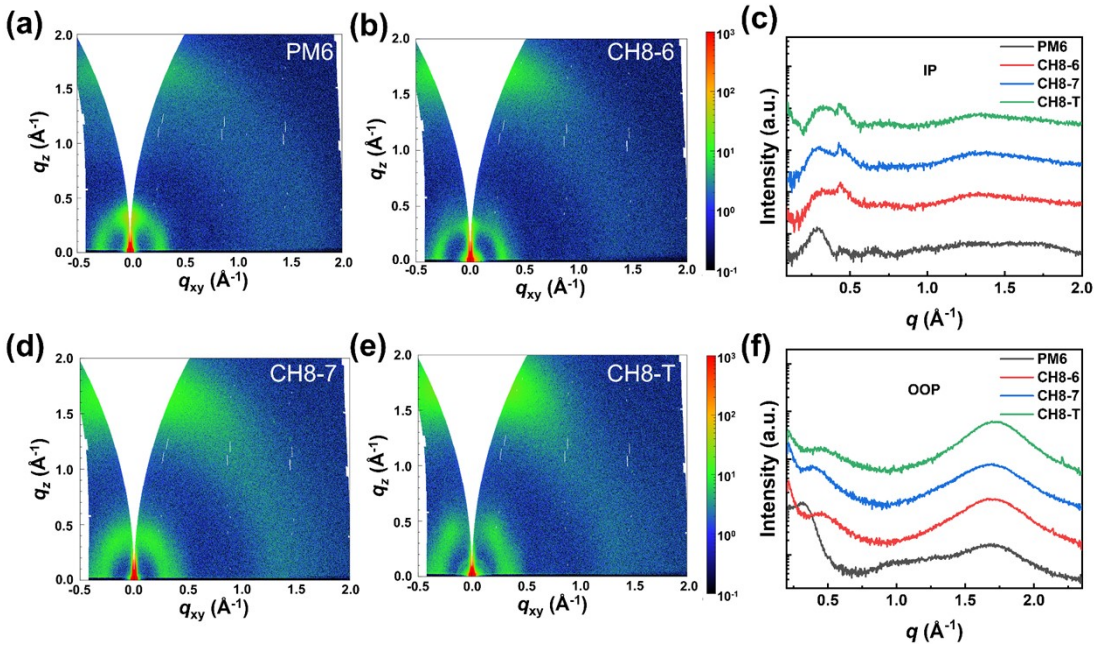

Figure S4. 2D GIWAXS patterns of (a) PM6 neat film, (b) CH8-6 neat film and (d) CH8-7 neat film and (e) CH8-T neat film, respectively; (c) Line cuts of GIWAXS images of the neat films in the in-plane (IP) direction; (f) Line cuts of GIWAXS images of the neat films in the out-of-plane (OOP) direction.

Table S9. GIWAXS measurement performance parameters of the related films in the out-of-plane (OOP) direction.

Film	Lamellar stacking (100)				π-π stacking (010)			
	q (Å^{-1})	d_1 (Å)	FWHM (Å^{-1})	CL[a] (Å)	*q* (Å^{-1})	d_1 (Å)	FWHM (Å^{-1})	CL[a] (Å)
PM6	0.320	19.63	0.160	35.34	1.677	3.75	0.462	12.24
CH8-6	0.455	13.81	0.236	23.96	1.691	3.72	0.347	16.30
CH8-7	0.388	16.19	0.202	27.99	1.677	3.75	0.356	15.88
CH8-T	0.467	13.45	0.257	22.00	1.714	3.66	0.338	16.73
PM6:CH8-6	0.267	23.53	0.179	31.59	1.723	3.65	0.298	18.98
PM6:CH8-7	0.309	20.33	0.139	40.68	1.698	3.70	0.330	17.14
PM6:CH8-T	-	-	-	-	1.729	3.63	0.286	19.77
PM6:CH8-6:L8-BO	0.290	21.67	0.142	39.82	1.728	3.64	0.277	20.41

[a]CL=0.9*2π/FWHM

Table S10. GIWAXS measurement performance parameters of the related films in the in-plane (IP) direction.

Film	Lamellar stacking (100)			
	Location ($Å^{-1}$)	d (Å)	FWHM ($Å^{-1}$)	CL[a] (Å)
PM6	0.287	21.86	0.099	57.12
CH8-6	0.315	19.94	0.207	27.32
CH8-7	0.307	20.46	0.157	36.02
CH8-T	0.325	19.93	0.289	19.57
PM6:CH8-6	0.304	20.69	0.085	66.83
PM6:CH8-7	0.297	21.16	0.072	78.54
PM6:CH8-T	0.294	21.37	0.079	71.58
PM6:CH8-6:L8-BO	0.307	20.46	0.058	97.50

[a]CL=0.9*2π/FWHM

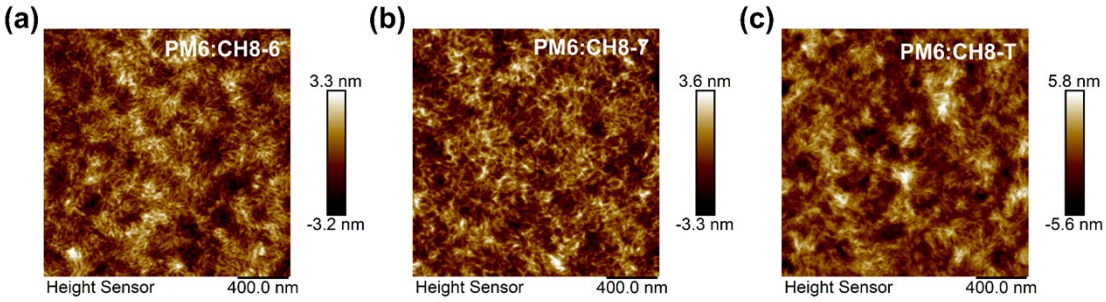

Figure S5. AFM height image of (a) PM6:CH8-6, (b) PM6:CH8-7 and (c) PM6:CH8-T, respectively.

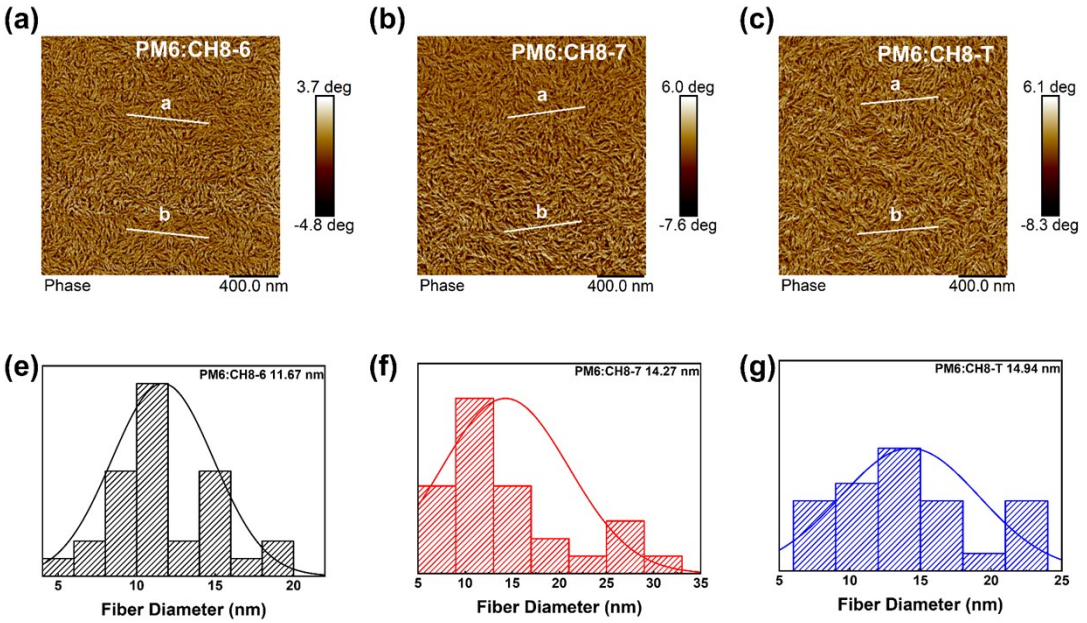

Figure S6. (a, b, c) AFM phase images of PM6:CH8-6, PM6:CH8-7 and PM6:CH8-T blend films; (d, e, f) The statistical distribution of the fiber diameter for PM6:CH8-6, PM6:CH8-7 and PM6:CH8-T blend films.

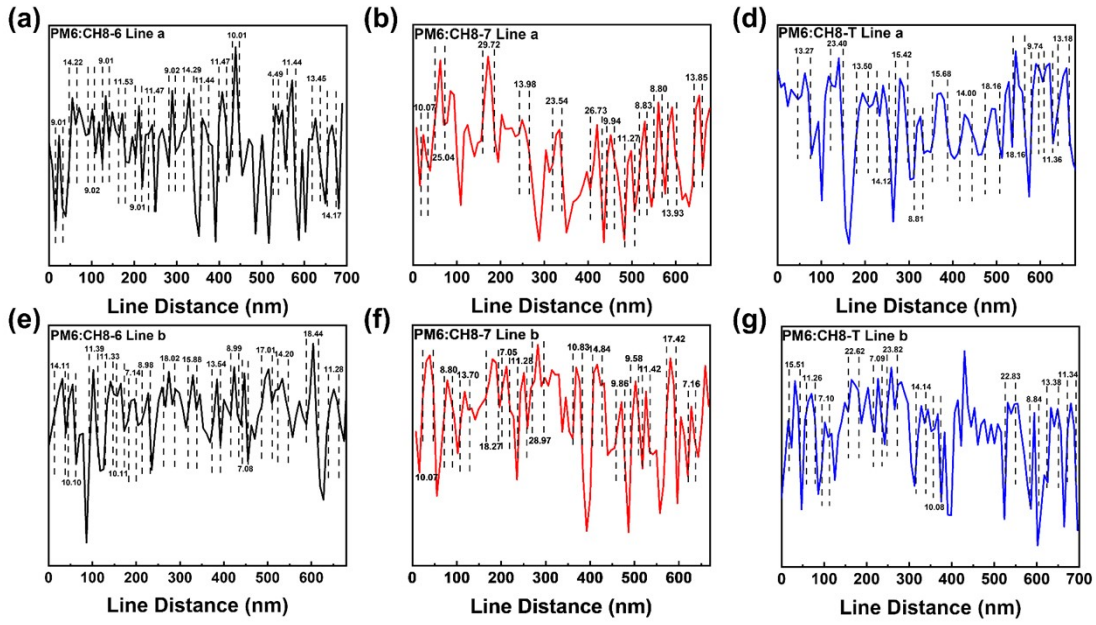

Figure S7. (a, b, c) The line a profile to obtain the fiber width form the AFM phase images of PM6:CH8-6, PM6:CH8-7 and PM6:CH8-T blend films; (d,e,f) The line b profile to obtain the fiber width form the AFM phase images of PM6:CH8-6, PM6:CH8-7 and PM6:CH8-T blend films.

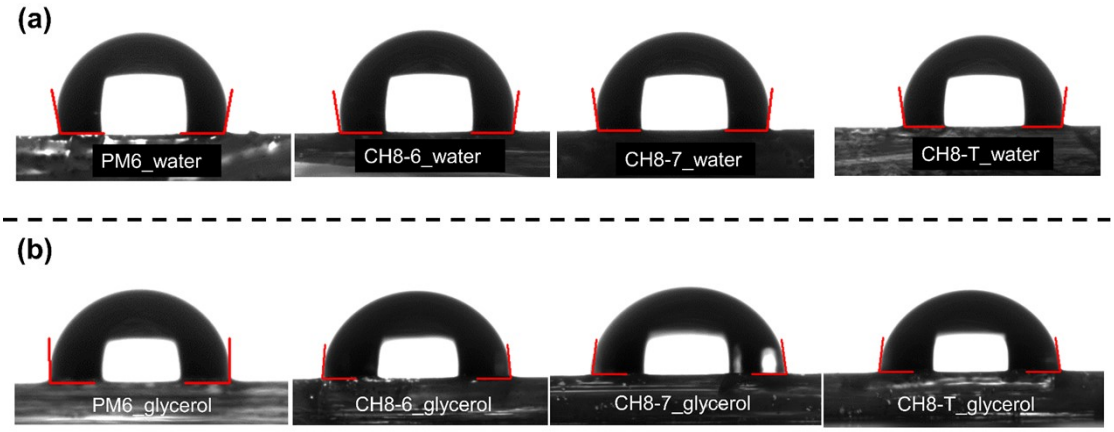

Figure S8. (a) Water droplet contact angles of PM6:CH8-6, PM6:CH8-7 and PM6:CH8-T; (b) Glycerol droplet contact angles of PM6:CH8-6, PM6:CH8-7 and PM6:CH8-T.

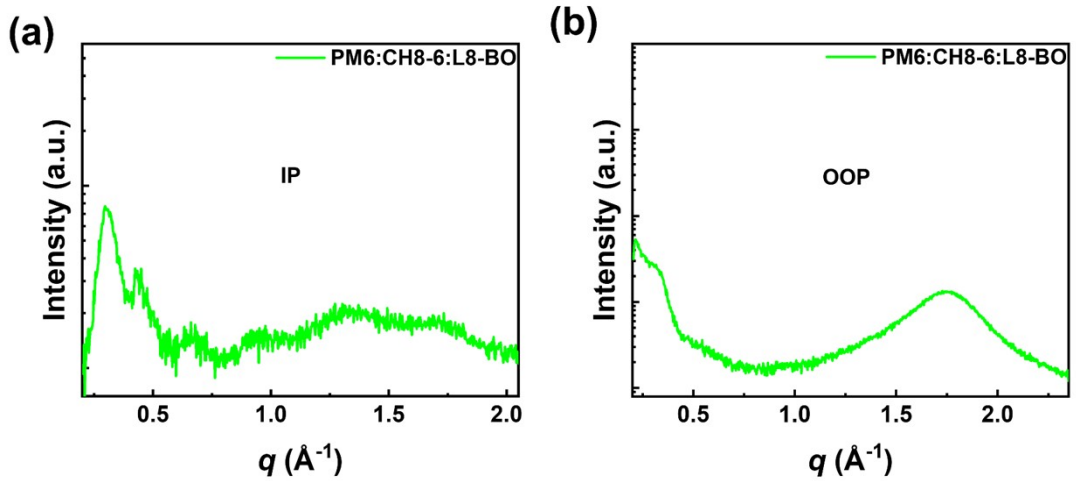

Figure S9. (a) Line cuts of GIWAXS images of the PM6:CH8-6:L8-BO blend film in the in-plane (IP) direction; (b) Line cuts of GIWAXS images of the PM6:CH8-6:L8-BO blend film in the out-of-plane (OOP) direction.

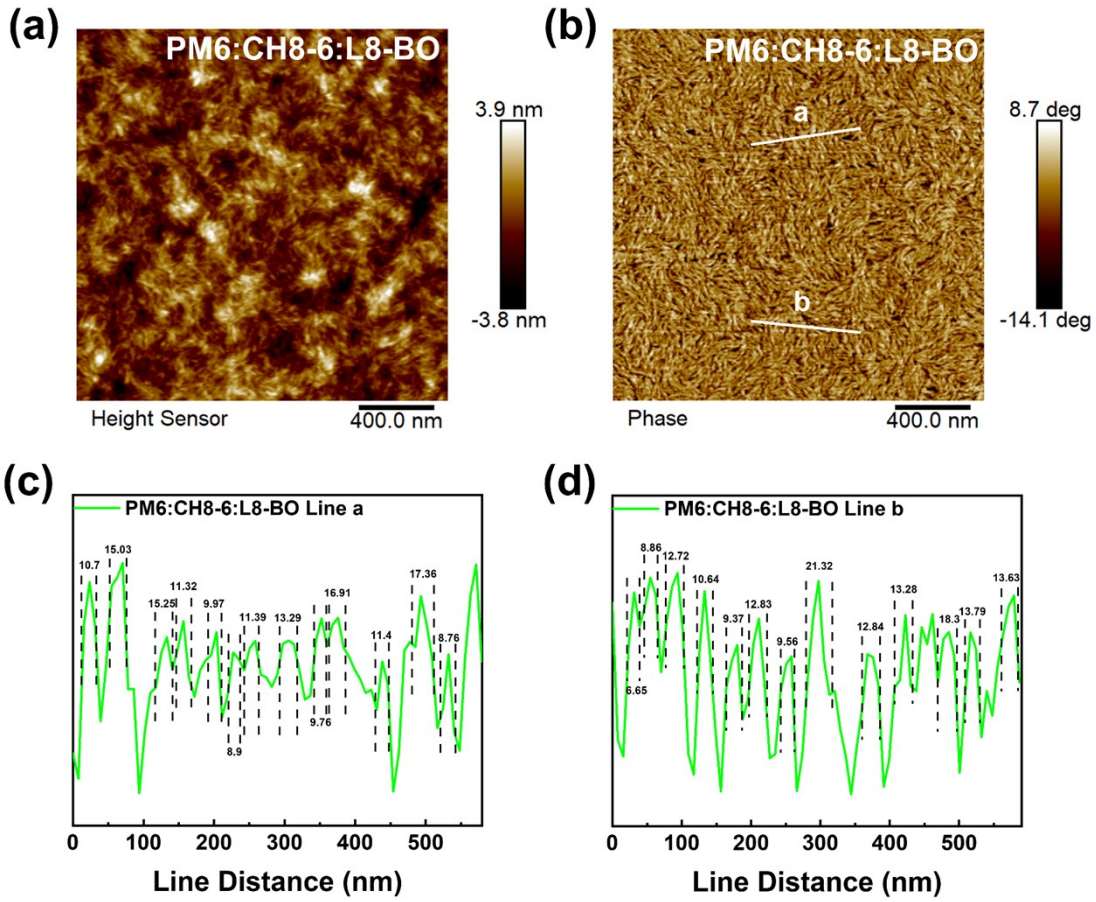

Figure S10. (a) AFM height image of PM6:CH8-6:L8-BO blend film; (b) AFM phase image of PM6:CH8-6:L8-BO blend film; (c) The line a profile to obtain the fiber width form the AFM phase images of PM6:CH8-6:L8-BO blend film; (d) The line b profile to obtain the fiber width form the AFM phase images of PM6:CH8-6:L8-BO blend film.

Table S11. Contact angle of neat films and miscibility parameters of blend films.

	CA of water (°)	CA of glycerol (°)	Surface Tension γ (mN m^{-1})	Relative $\chi_{PM6:A}$
PM6	100.48	93.03	20.6	-
CH8-6	98.64	84.83	25.0	0.213 K
CH8-7	97.41	84.63	25.6	0.271 K
CH8-T	97.48	83.15	26.3	0.348 K

Table S12. The photovoltaic parameters of flexible devices.

Active layer	V_{oc} (V)	J_{sc} (mA cm^{-2})	FF (%)	PCE (%)
PM6:CH8-6	0.881	25.27	72.81	16.2
PM6:CH8-7	0.903	23.82	73.35	15.8
PM6:CH8-T	0.865	25.34	72.37	15.9

Table S13. Summary of reported OSCs based on oligomeric acceptors.

Active layer	V_{oc} (V)	J_{sc} (mA cm^{-2})	FF (%)	PCE (%)	Ref.
PM6:*d*BTICγ-EH	0.92	21.43	73.28	14.48	1
PM6:*d*BTICγ-BO	0.91	20.97	70.26	13.42	1
PM6:*t*BTICγ-EH	0.90	21.25	68.76	13.16	1
PBQx-H-TF/ *d*BTICγ-BO	0.91	23.41	75.49	16.06	1
PM6:CH8	0.89	19.70	53.5	9.37	2
D18-Cl-B:4A-DFIC	0.84	22.47	77.4	15.76	3
D18-Cl-B:N3:4A-DFIC	0.86	28.35	76.6	18.60	3
PM6:QM1	0.91	25.23	74.01	17.05	4
PM6:QM2	0.91	25.42	70.50	16.36	4
PM6:2BTP-2F-T	0.91	25.50	78.28	18.19	5
PBDB-T:OY2	0.84	24.37	71.79	14.69	6
PBDB-T:OY3	0.84	23.76	74.58	14.87	6
PBDB-T:OY4	0.81	24.39	74.69	14.82	6
PM6:DY1	0.87	25.67	73.24	16.46	7
PM6:DY2	0.87	26.60	76.85	17.85	7
PM6:DY3	0.87	26.20	76.21	17.33	7
D18:DY-T	0.95	22.57	72.47	15.52	8

D18:DY-TF	0.95	24.36	72.87	16.77	8
D18-DYF-TF	0.94	25.82	75.30	18.26	8
PM6:DYBO	0.97	24.62	75.8	18.08	9
PM6:DYT	0.94	24.08	76.0	17.30	10
PM6:DYV	0.93	25.64	78.0	18.60	10
PM6:DYTVT	0.93	24.82	74.0	17.68	10
PM6:CH-D1	0.95	23.90	73.20	16.62	11
PM6:PZC24:CH-D1	0.95	24.23	75.25	17.40	11
PM6:CH8-0	0.94	22.61	72.1	15.26	12
PM6:CH8-1	0.92	24.89	74.2	17.03	12
PM6:CH8-2	0.93	24.24	74.9	16.84	12
PM6:EV-i	0.90	26.60	76.56	18.27	13
PM6:EV-o	0.96	6.20	42.13	2.50	13
PM6:DYV	0.91	25.97	76.22	18.01	14
PM6:DYVC	0.92	24.87	73.86	16.81	14
PM6:DYTVT	0.94	22.90	68.15	14.59	14
PM6:DYB	0.94	20.51	67.41	12.98	14
PM6:DYID	0.91	12.90	47.00	5.53	14
PM6:TDY-α	0.84	25.9	74.3	16.2	15
PM6:TDY-β	0.86	26.9	78.0	18.1	15
D18:DYA-I	0.94	25.67	78	18.83	16
D18:DYA-IO	0.95	24.29	76	17.54	16
D18:DYA-O	0.96	23.32	73	16.45	16
PM6:*d*T9TBO	0.99	9.49	62.09	5.84	17
PM6:Y6:*d*T9TBO	0.88	27.17	77.26	18.41	17
PM6:DYT	0.94	24.89	74	17.29	18

PM6:TVT	0.96	25.07	75	18.15	18
PM6:Tri-Y6-OD	0.92	25.30	77.8	18.03	19
PM6:Tri-DT	0.94	23.89	77.4	17.44	19
PM6:BT-BTz-BT	0.93	23.61	74.3	16.28	19
PM6:BO-C11-BO	0.95	21.05	73.4	14.69	19
PM6:DIBP3F-Se	0.92	25.92	76.1	18.09	20
PM6:DIBP3F-S	0.90	24.86	72.0	16.11	20
D18:N3:DOY-TVT	0.86	28.21	79.38	19.20	21
PM6:RCM	0.98	22.7	63.8	14.2	22
PM6:DBTP-C3	0.99	17.4	70.7	12.2	22
D18:DP-BTP	0.96	22.73	69.10	15.08	23
D18:N3:DP-BTP	0.87	27.95	78.50	19.07	23
PM6:CH8-3	0.92	24.44	77.0	17.22	24
PM6:CH8-4	0.89	26.05	75.5	17.58	24
PM6:CH8-5	0.90	24.75	75.2	16.79	24
PM6:DY-P2EH	0.91	24.03	78.58	17.09	25
PM6:FY-P2EH:BYP-eC9	0.87	27.19	80.61	19.09	25
PM6:L8-BO:DY-TF	0.91	26.93	78.50	19.13	26
PM6:Y6:DT-19	0.86	27.6	71.7	17.1	27
PM6:BO-4F:DT-19	0.85	27.0	74.4	17.0	27
PM6:L8-BO:DT-19	0.90	27.8	73.8	18.4	27
PM6:BO-4Cl:DT-19	0.86	27.6	70.4	16.7	27
PM6:Dimer-QX	0.93	22.57	69.26	14.59	28
PM6:Dimer-2CF	0.90	26.39	80.03	19.02	28
PM6:G-Dimer	0.90	24.39	78.95	17.41	29
PM6:G-Trimer	0.90	26.75	79.30	19.01	29

PBQx-H-TF:dBTIC-δV-BO	0.96	20.67	66.06	13.15	30
PBQx-H-TF:dBTIC-γV-BO	0.91	24.52	76.58	17.14	30
PBQx-H-TF:dBTIC-γV-BO-2Cl	0.87	24.65	74.71	16.04	30
D18:DYT	0.95	24.16	75.0	17.20	31
D18:TYT-L	0.97	24.19	75.0	17.47	31
D18:TVT-S	0.96	25.18	77.0	18.61	31
PM6:DBT	0.95	24.12	72.39	16.53	32
PM6:TBT	0.94	24.63	78.07	18.04	32
D18:2Y-wing	0.85	27.66	75.4	17.73	33
D18:2Y-core	0.86	10.58	61.5	5.63	33
D18:2Y-end	0.95	22.39	68.5	14.46	33
D18:BS3TSe-4F:2Y-wing	0.85	29.35	77.0	19.13	33
D18: BS3TSe-4F:2Y-core	0.85	27.95	75.1	17.80	33
BS3TSe-4F:2Y-end	0.85	28.12	76.1	18.17	33
PM6:BT-DL	0.94	25.52	77.1	18.49	34
PM6:B-DL	0.95	18.56	52.1	9.17	34
PM6:Tri-BT	0.93	25.49	74.9	17.81	35
PM6:Tri-Qx	0.94	25.28	77.5	18.33	35
PM6:TQT	0.94	25.78	76.1	18.52	35
PM6:L8-BO:TQT	0.89	26.75	80.7	19.15	35
PM6:HDY-m-TAT	0.92	23.22	67.8	14.42	36
PM6:FDY-m-TAT	0.91	26.47	74.7	18.07	36
PM6:HDY-o-TAT	0.93	23.07	70.4	15.23	36
PM6:FDY-o-TAT	0.91	25.14	73.6	16.91	36
PBQx-H-TF/dBTIC-Se-HD	0.93	22.41	63.3	13.22	37
PBQx-H-TF/dBSeIC-Se-OD	0.93	23.08	69.50	14.91	37

PBQx-H-TF/dBSeIC2IC-Se-OD	0.89	26.20	72.90	17.03	37
PM6:DYV-Cl	0.92	22.93	69.00	14.52	38
PM6:DYV-2Cl	0.91	22.50	70.33	13.36	38
PM6:DYV-γ-2Cl	0.92	23.32	73.73	15.54	38
D18:DBY-2Cl	0.93	20.76	68.76	13.23	39
D18:DTY-2Cl	0.91	26.20	75.46	18.06	39
D18/BTP-eC9:*d*BTP-ThC2	0.87	27.41	75.59	18.06	40
D18/BTP-eC9:*d*BTP-ThC4	0.88	28.29	76.94	19.09	40
D18/BTP-eC9:*d*BTP-ThC6	0.88	27.72	77.05	18.73	40
D18/L8-BO:*d*BTP-ThC4	0.92	26.30	79.60	19.16	40
PM6:CH8-6	0.891	26.23	77.8	18.2	This work
PM6:CH8-6:L8-BO	0.884	27.63	78.6	19.2	This work

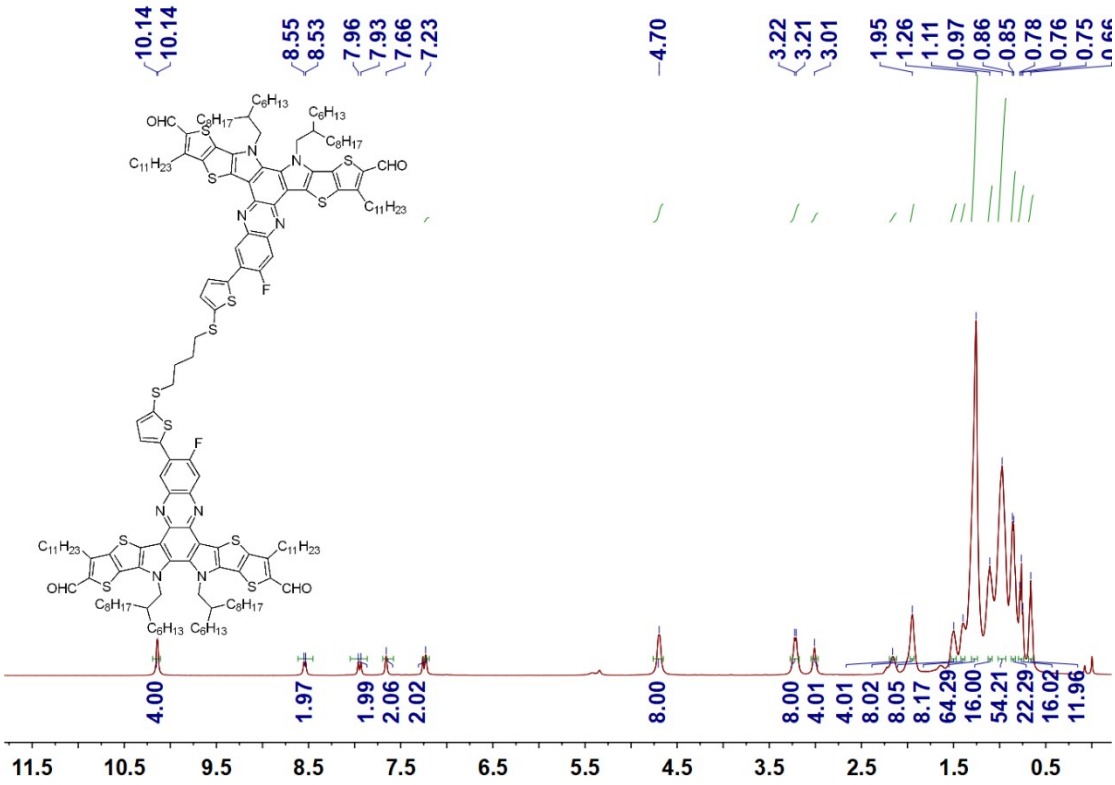

Figure S11. ^{1}H NMR spectrum of compound **3** at 300K in $CDCl_3$.

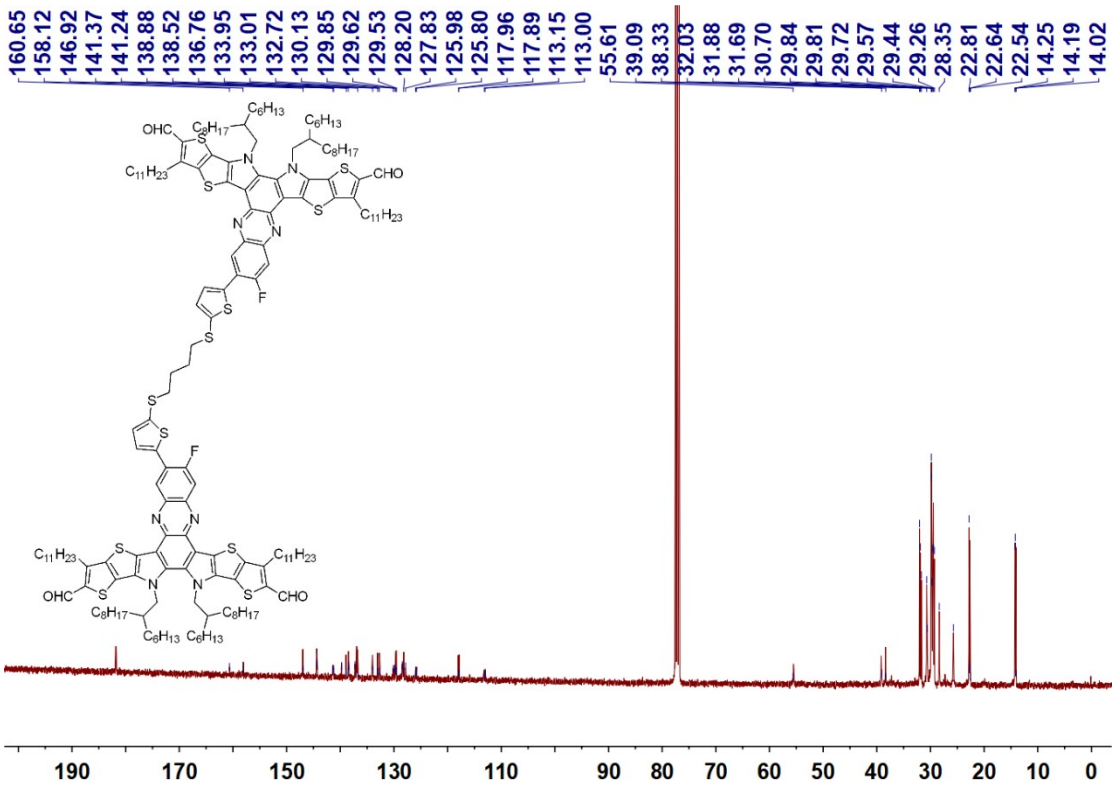

Figure S12. ^{13}C NMR spectrum of compound **3** at 300K in $CDCl_3$.

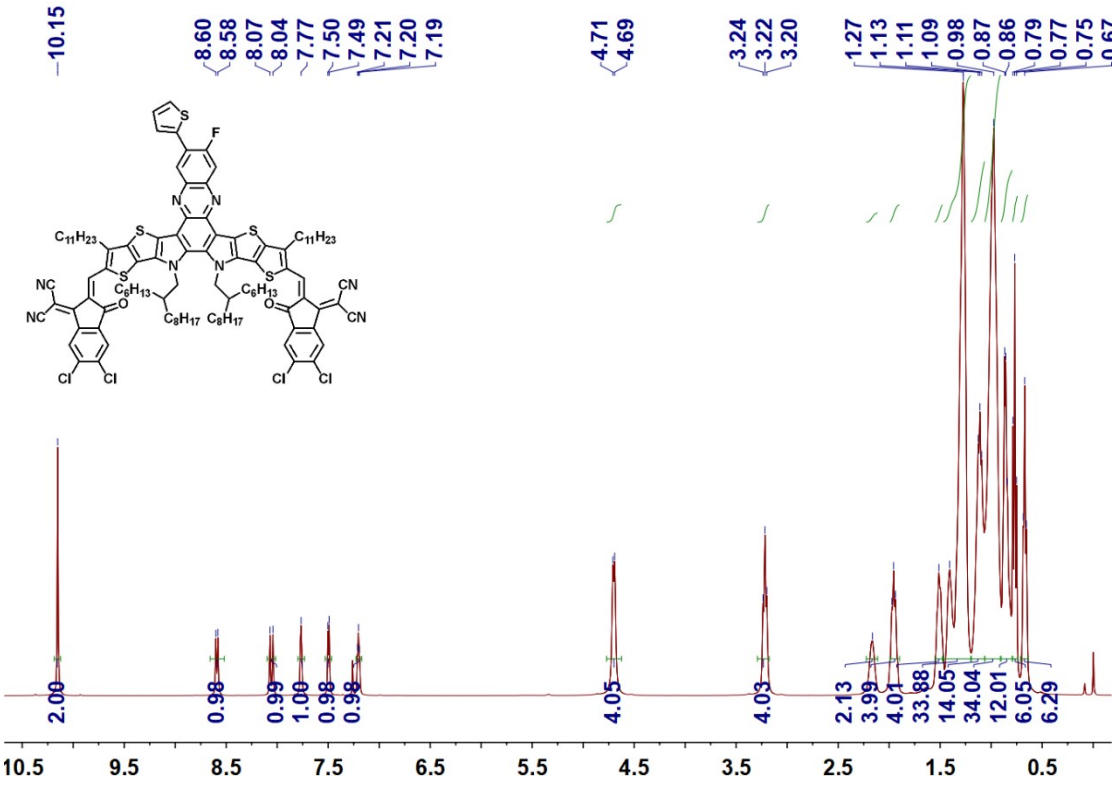

Figure S13. ^{1}H NMR spectrum of compound **4** at 300K in $CDCl_3$.

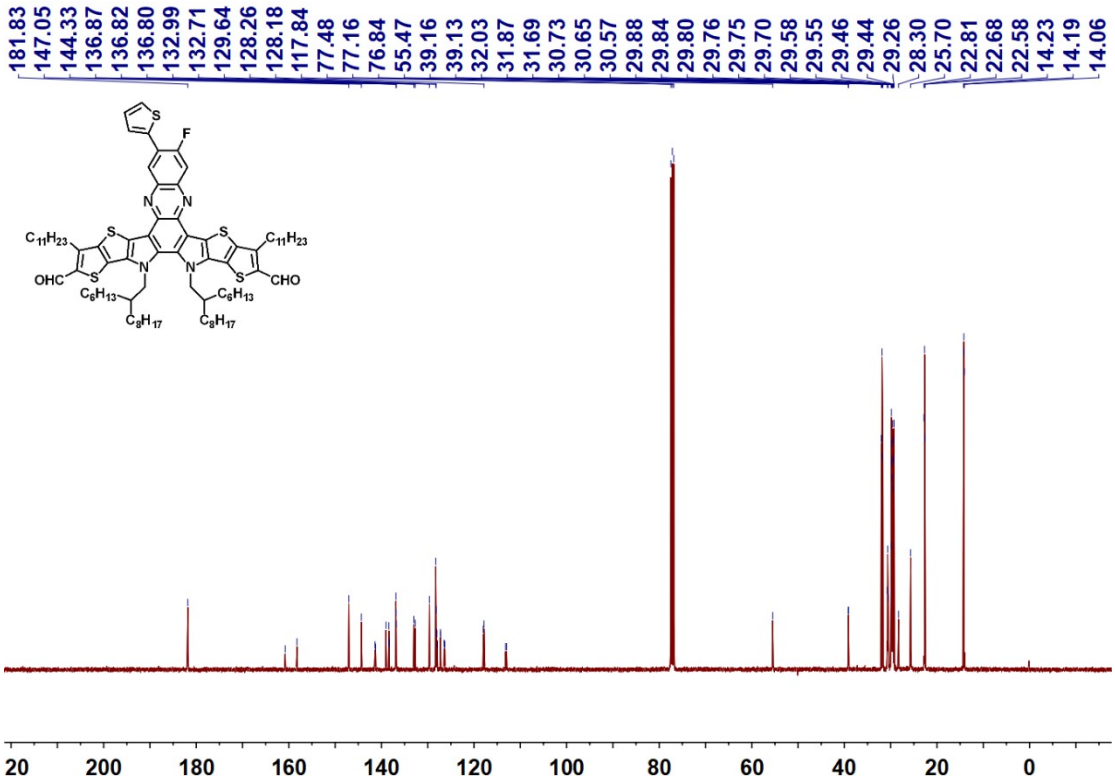

Figure S14. ^{13}C NMR spectrum of compound **4** at 300K in $CDCl_3$.

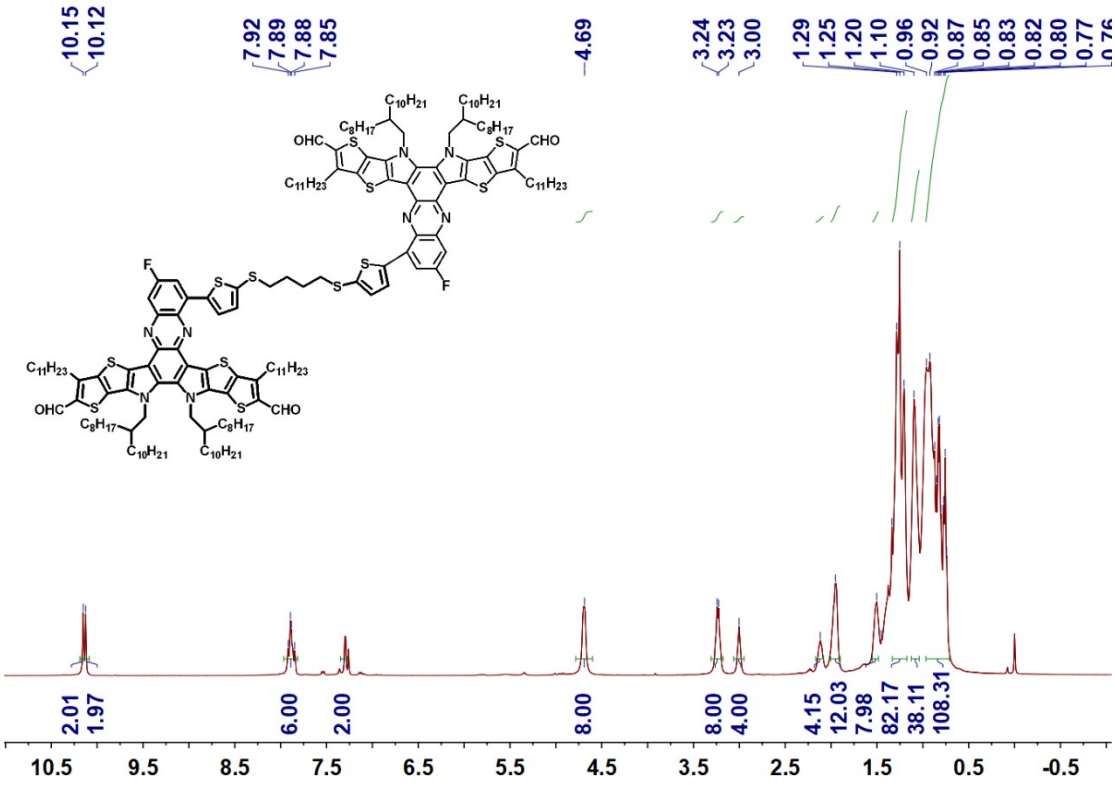

Figure S15. ^{1}H NMR spectrum of compound **5** at 300K in $CDCl_3$.

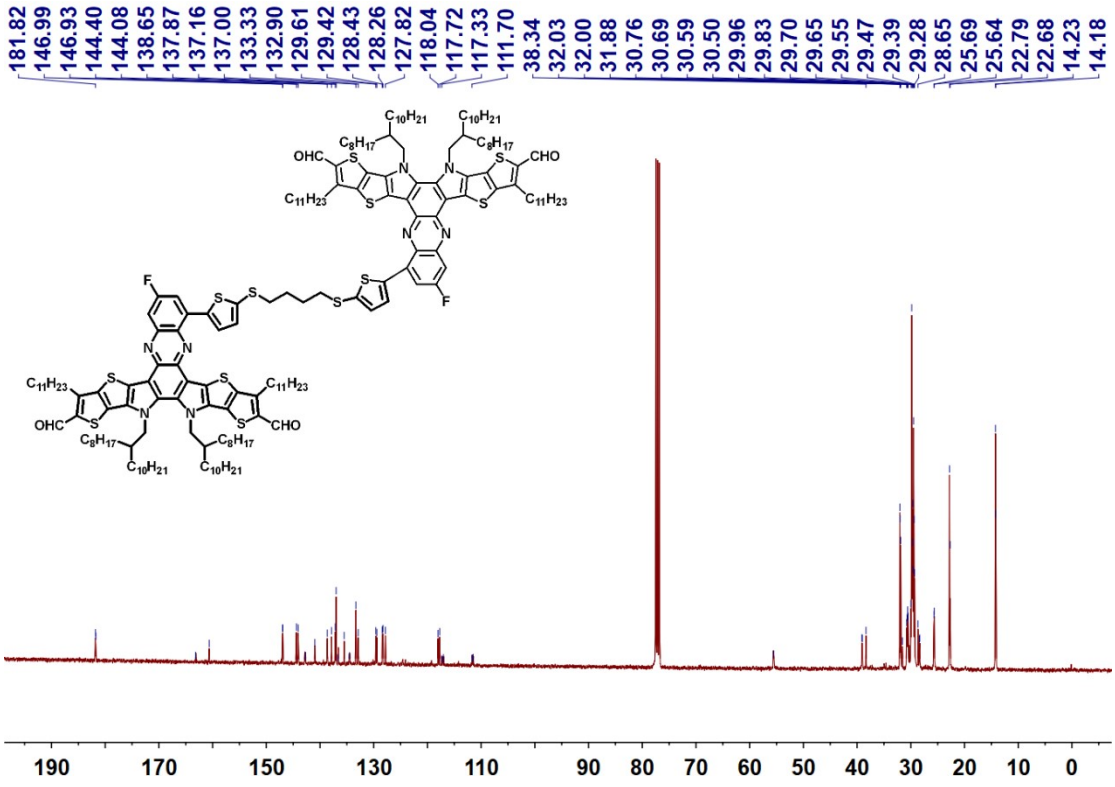

Figure S16. ^{13}C NMR spectrum of compound **5** at 300K in $CDCl_3$.

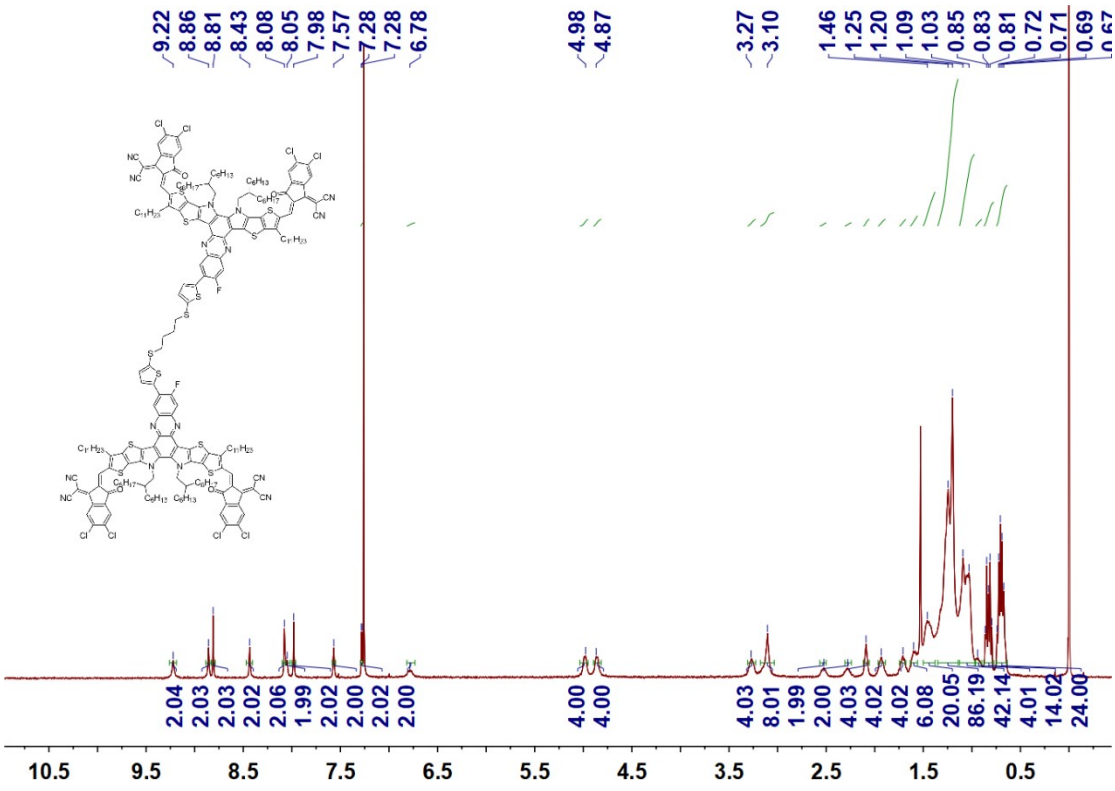

Figure S17. ^{1}H NMR spectrum of compound **CH8-6** at 300K in $CDCl_3$.

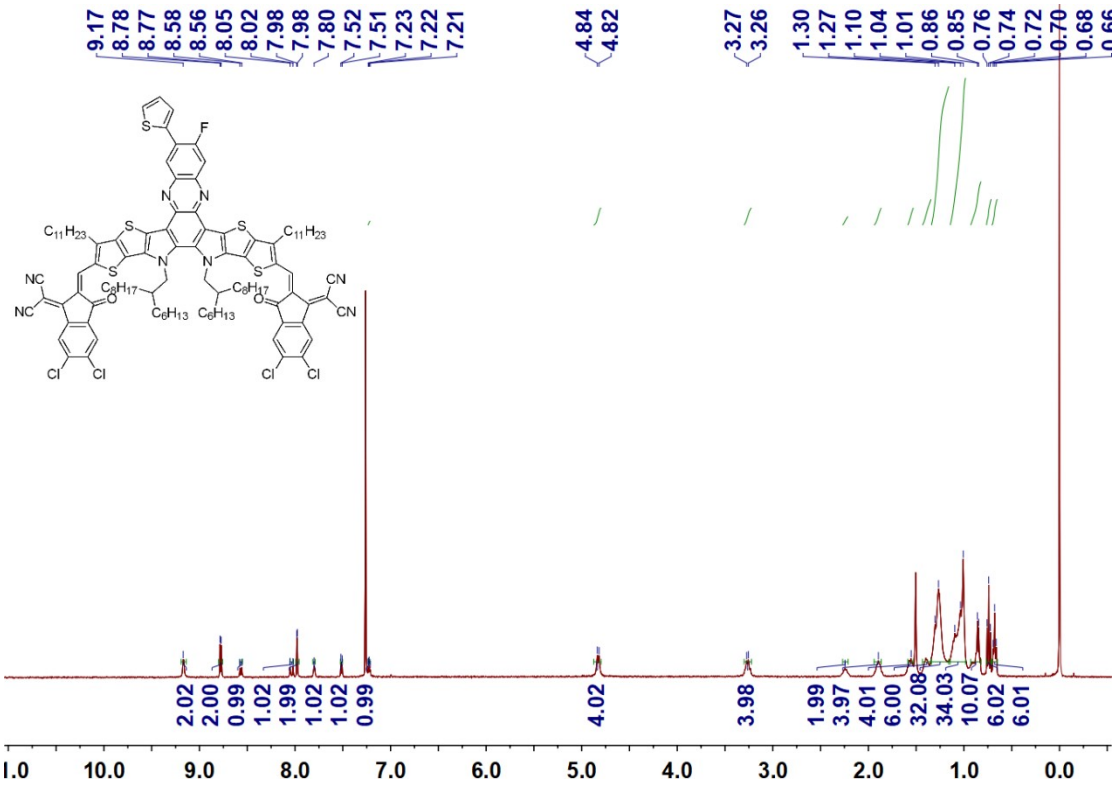

Figure S18. ^{1}H NMR spectrum of compound **CH8-T** at 300K in $CDCl_3$.

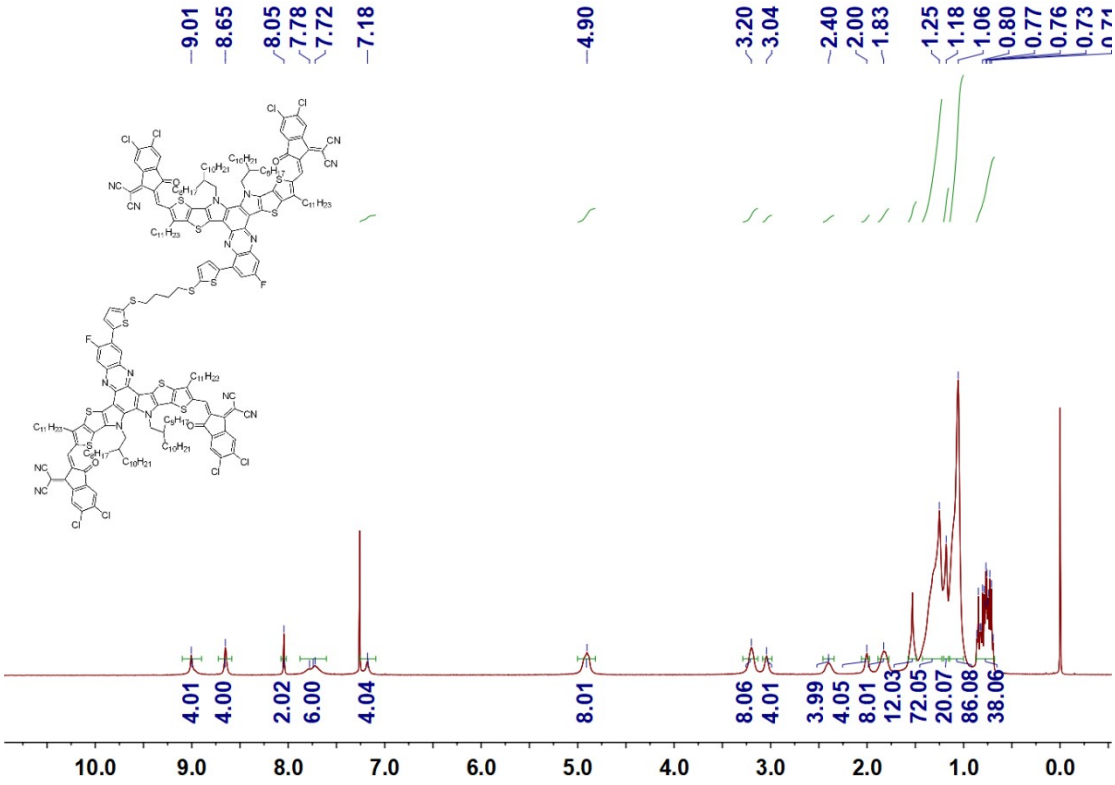

Figure S19. ^{1}H NMR spectrum of compound **CH8-7** at 300K in $CDCl_3$.

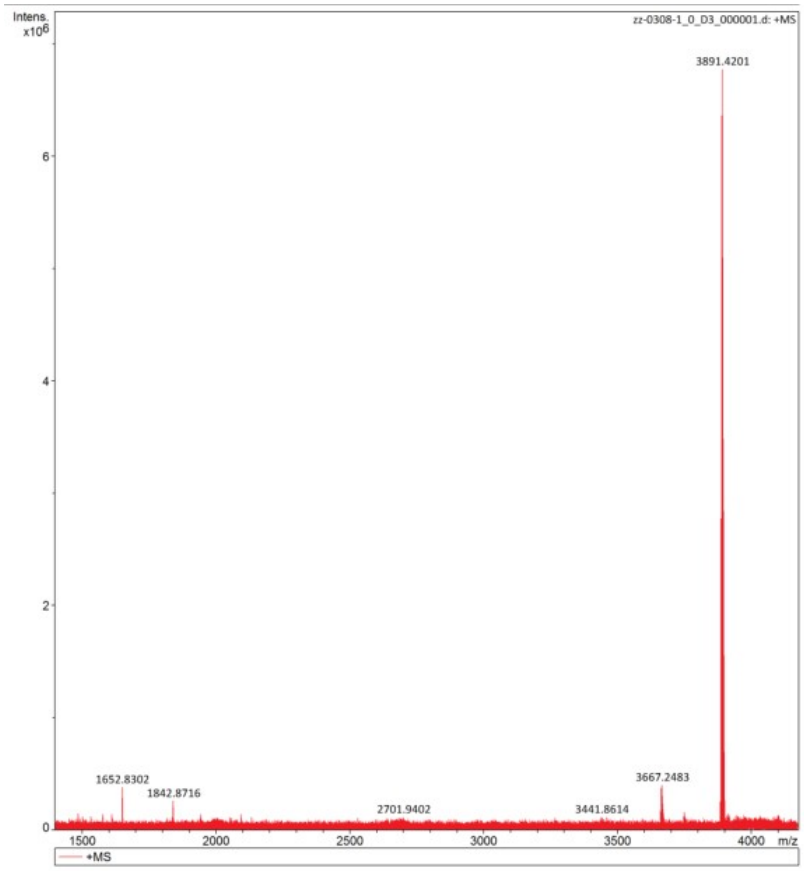

Figure S20. HRMS spectrum of compound **CH8-6**.

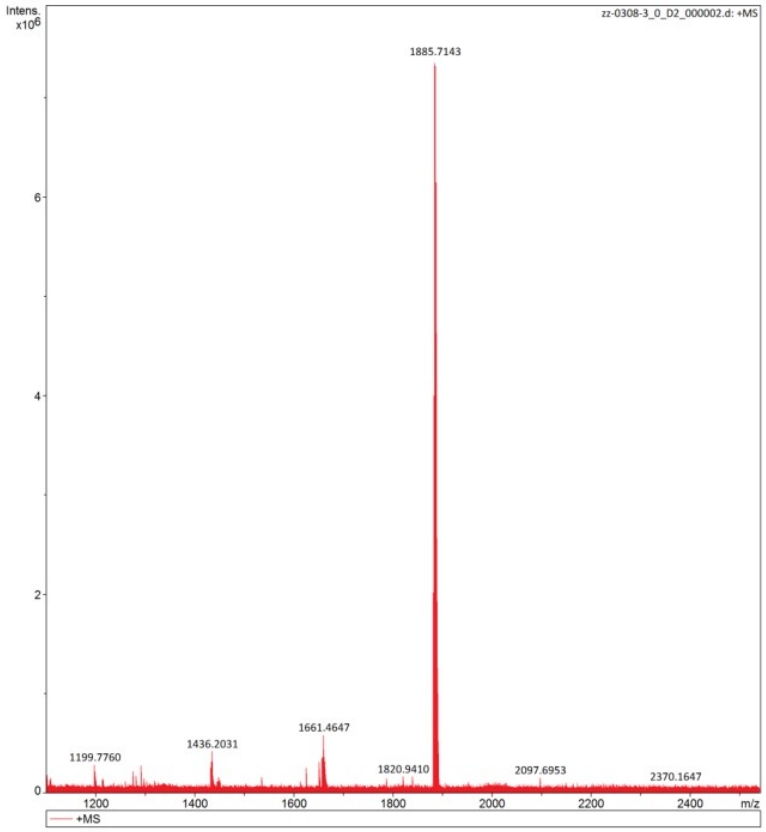

Figure S21. HRMS spectrum of compound **CH8-T**.

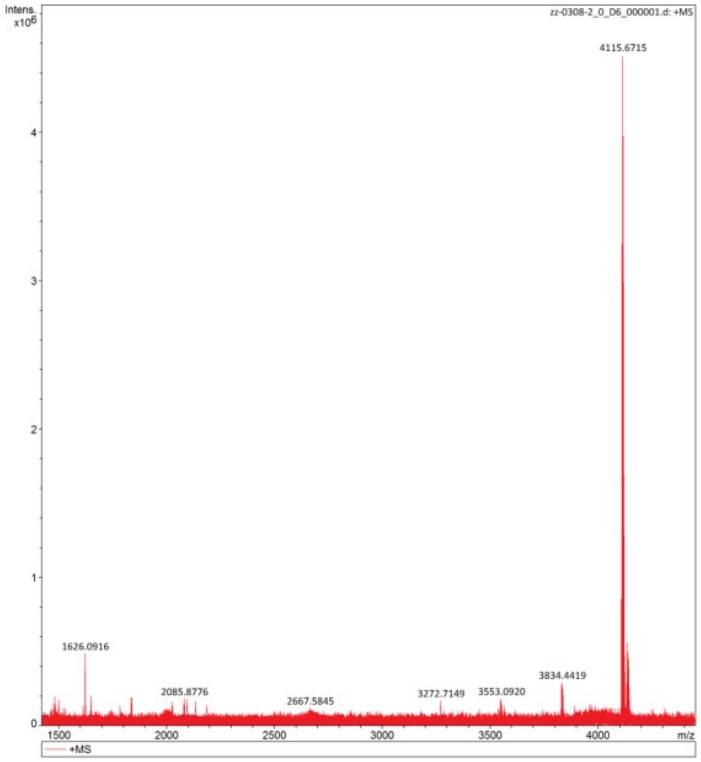

Figure S22. HRMS spectrum of compound **CH8-7**.

References

1. H. Wang, C. Cao, H. Chen, H. Lai, C. Ke, Y. Zhu, H. Li and F. He, *Angew. Chem. Int. Ed.*, 2022, **61**, 202201844.
2. H. Chen, X. Cao, X. Xu, C. Li, X. Wan, Z. Yao and Y. Chen, *Chinese J. Polym. Sci.* , 2022, **40**, 921-927.
3. X. Meng, M. Li, K. Jin, L. Zhang, J. Sun, W. Zhang, C. Yi, J. Yang, F. Hao, G. W. Wang, Z. Xiao and L. Ding, *Angew. Chem. Int. Ed.*, 2022, **61**, e202207762.
4. W. Liu, J. Yuan, C. Zhu, Q. Wei, S. Liang, H. Zhang, G. Zheng, Y. Hu, L. Meng, F. Gao, Y. Li and Y. Zou, *Sci. China: Chem.*, 2022, **65**, 1374-1382.
5. L. Zhang, Z. Zhang, D. Deng, H. Zhou, J. Zhang and Z. Wei, *Adv. Sci.*, 2022, **9**, 2202513.
6. Y. Liang, D. Zhang, Z. Wu, T. Jia, L. Lüer, H. Tang, L. Hong, J. Zhang, K. Zhang, C. J. Brabec, N. Li and F. Huang, *Nat. Energy*, 2022, **7**, 1180-1190.

7. S. Li, R. Zhang, M. Zhang, J. Yao, Z. Peng, Q. Chen, C. Zhang, B. Chang, Y. Bai, H. Fu, Y. Ouyang, C. Zhang, J. A. Steele, T. Alshahrani, M. B. J. Roeffaers, E. Solano, L. Meng, F. Gao, Y. Li and Z. G. Zhang, *Adv. Mater.*, 2023, **35**, 2206563.
8. X. Gu, Y. Wei, N. Yu, J. Qiao, Z. Han, Q. Lin, X. Han, J. Gao, C. Li, J. Zhang, X. Hao, Z. Wei, Z. Tang, Y. Cai, X. Zhang and H. Huang, *CCS Chemistry*, 2023, **5**, 2576-2588.
9. C. Sun, J.-W. Lee, C. Lee, D. Lee, S. Cho, S.-K. Kwon, B. J. Kim and Y.-H. Kim, *Joule*, 2023, **7**, 416-430.
10. J.-W. Lee, C. Sun, C. Lee, Z. Tan, T. N.-L. Phan, H. Jeon, D. Jeong, S.-K. Kwon, Y.-H. Kim and B. J. Kim, *ACS Energy Lett.*, 2023, **8**, 1344-1353.
11. Z. Li, Z. Zhang, H. Chen, Y. Zhang, Y. Q. Q. Yi, Z. Liang, B. Zhao, M. Li, C. Li, Z. Yao, X. Wan, B. Kan and Y. Chen, *Adv. Energy Mater.* , 2023, **13**, 230030.
12. H. Chen, Z. Zhang, P. Wang, Y. Zhang, K. Ma, Y. Lin, T. Duan, T. He, Z. Ma, G. Long, C. Li, B. Kan, Z. Yao, X. Wan and Y. Chen, *Energy Environ. Sci*, 2023, **16**, 1773-1782.
13. H. Zhuo, X. Li, J. Zhang, S. Qin, J. Guo, R. Zhou, X. Jiang, X. Wu, Z. Chen, J. Li, L. Meng and Y. Li, *Angew. Chem., Int. Ed.*, 2023, **62**, e202303551.
14. H. Fu, M. Zhang, Y. Zhang, Q. Wang, Z. Xu, Q. Zhou, Z. Li, Y. Bai, Y. Li and Z. G. Zhang, *Angew. Chem., Int. Ed.*, 2023, **62**, e202306303.
15. Y. Bai, Z. Zhang, Q. Zhou, H. Geng, Q. Chen, S. Kim, R. Zhang, C. Zhang, B. Chang, S. Li, H. Fu, L. Xue, H. Wang, W. Li, W. Chen, M. Gao, L. Ye, Y. Zhou, Y. Ouyang, C. Zhang, F. Gao, C. Yang, Y. Li and Z. G. Zhang, *Nat. Commun.*, 2023, **14**, 2926.
16. C. Sun, J. W. Lee, Z. Tan, T. N. L. Phan, D. Han, H. G. Lee, S. Lee, S. K. Kwon, B. J. Kim and Y. H. Kim, *Adv. Energy Mater.*, 2023, **13**, e2301283.
17. F. Qi, Y. Li, R. Zhang, F. R. Lin, K. Liu, Q. Fan and A. K. Jen, *Angew. Chem., Int. Ed.*, 2023, **62**, e202303066.

18. J.-W. Lee, C. Sun, T. N.-L. Phan, D. C. Lee, Z. Tan, H. Jeon, S. Cho, S.-K. Kwon, Y.-H. Kim and B. J. Kim, *Energy Environ. Sci*, 2023, **16**, 3339-3349.
19. C. Zhang, J. Song, J. Xue, S. Wang, Z. Ge, Y. Man, W. Ma and Y. Sun, *Angew. Chem. Int. Ed.*, 2023, **62**, e202308595.
20. J. Wu, Z. Ling, L. R. Franco, S. Y. Jeong, Z. Genene, J. Mena, S. Chen, C. Chen, C. M. Araujo, C. F. N. Marchiori, J. Kimpel, X. Chang, F. H. Isikgor, Q. Chen, H. Faber, Y. Han, F. Laquai, M. Zhang, H. Y. Woo, D. Yu, T. D. Anthopoulos and E. Wang, *Angew. Chem. Int. Ed.*, 2023, **62**, e202302888.
21. W. Song, Q. Ye, S. Yang, L. Xie, Y. Meng, Z. Chen, Q. Gu, D. Yang, J. Shi and Z. Ge, *Angew. Chem. Int. Ed.*, 2023, **62**, e202310034.
22. W. Liu, H. Zhang, S. Liang, T. Wang, S. He, Y. Hu, R. Zhang, H. Ning, J. Ren, A. Bakulin, F. Gao, J. Yuan and Y. Zou, *Angew. Chem. Int. Ed.*, 2023, **62**, e202311645.
23. X. Liu, Z. Zhang, C. Wang, C. Zhang, S. Liang, H. Fang, B. Wang, Z. Tang, C. Xiao and W. Li, *Angew. Chem. Int. Ed.*, 2024, **63**, e202316039.
24. H. Chen, B. Kan, P. Wang, W. Feng, L. Li, S. Zhang, T. Chen, Y. Yang, T. Duan, Z. Yao, C. Li, X. Wan and Y. Chen, *Angew. Chem. Int. Ed.*, 2023, **62**, e202307962.
25. M. Zhang, B. Chang, R. Zhang, S. Li, X. Liu, L. Zeng, Q. Chen, L. Wang, L. Yang, H. Wang, J. Liu, F. Gao and Z. G. Zhang, *Adv. Mater.*, 2024, **36**, e2308606.
26. Y. Wei, Y. Cai, X. Gu, G. Yao, Z. Fu, Y. Zhu, J. Yang, J. Dai, J. Zhang, X. Zhang, X. Hao, G. Lu, Z. Tang, Q. Peng, C. Zhang and H. Huang, *Adv. Mater.*, 2023, DOI: 10.1002/adma.202304225, e2304225.
27. J. Wan, T. Wang, R. Sun, X. Wu, S. Wang, M. Zhang and J. Min, *Adv. Mater.*, 2023, **35**, e2302592.
28. M. Lv, Q. Wang, J. Zhang, Y. Wang, Z. G. Zhang, T. Wang, H. Zhang, K. Lu, Z. Wei and D. Deng, *Adv. Mater.*, 2024, **36**, e2310046.

29. C. Wang, X. Ma, Y.-f. Shen, D. Deng, H. Zhang, T. Wang, J. Zhang, J. Li, R. Wang, L. Zhang, Q. Cheng, Z. Zhang, H. Zhou, C. Tian and Z. Wei, *Joule*, 2023, **7**, 2386-2401.

30. P. Tan, H. Chen, H. Wang, X. Lai, Y. Zhu, X. Shen, M. Pu, H. Lai, S. Zhang, W. Ma and F. He, *Adv. Funct. Mater.*, 2023, **34**, e2305608.

31. J. W. Lee, C. Sun, J. Lee, D. J. Kim, W. J. Kang, S. Lee, D. Kim, J. Park, T. N. L. Phan, Z. Tan, F. S. Kim, J. Y. Lee, X. Bao, T. S. Kim, Y. H. Kim and B. J. Kim, *Adv. Energy Mater.*, 2024, **14**, e2303872.

32. W. Liu, X. Xu, S. He, R. Sun, Q. Chen, J. Min, Z. Zhang, J. Yuan, Y. Li and Y. Zou, *Macromolecules*, 2023, **56**, 8623-8631.

33. F. Yi, M. Xiao, Y. Meng, H. Bai, W. Su, W. Gao, Z. F. Yao, G. Qi, Z. Liang, C. Jin, L. Tang, R. Zhang, L. Yan, Y. Liu, W. Zhu, W. Ma and Q. Fan, *Angew. Chem., Int. Ed.*, 2024, **63**, e202319295.

34. H. Fu, Q. Wang, Q. Chen, Y. Zhang, S. Meng, L. Xue, C. Zhang, Y. Yi and Z. G. Zhang, *Angew. Chem. Int. Ed.*, 2024, **63**, e202403005.

35. J. Liu, X. Duan, J. Song, C. Liu, J. Gao, M. H. Jee, Z. Tang, H. Y. Woo and Y. Sun, *Energy Environ. Sci.*, 2024, **17**, 3641-3650.

36. Y. Ding, W. A. Memon, D. Zhang, Y. Zhu, S. Xiong, Z. Wang, J. Liu, H. Li, H. Lai, M. Shao and F. He, *Angew. Chem. Int. Ed.*, 2024, **63**, e202403139.

37. M. Ou, S. Xiong, X. Shen, H. Lai, X. Lai, Y. Wang, H. Li and F. He, *Macromolecules*, 2024, **57**, 4167-4173.

38. X. Shen, S. Xiong, H. Lai, Y. Wang, H. Li, Z. Deng and F. He, *ACS Appl. Mater. Interfaces*, 2024, **16**, 27463-27469.

39. X. Shen, X. Lai, H. Lai, Y. Wang, H. Li, M. Ou and F. He, *Adv. Funct. Mater.*, 2024, DOI: 10.1002/adfm.202404919.

40. Y. Li, F. Qi, B. Fan, K. K. Liu, J. Yu, Y. Fu, X. Liu, Z. Wang, S. Zhang, G. Lu, X. Lu, Q. Fan, P. C. Y. Chow, W. Ma, F. R. Lin and A. K. Jen, *Adv. Mater.*, 2024, **36**, e2313393.